© 2023. Published by The Company of Biologists Ltd | Journal of Cell Science (2023) 136, jcs260380. doi:10.1242/jcs.260380

RESEARCH ARTICLE

SART3 associates with a post-splicing complex

Klára Klimešová[1,*,‡], Hana Petržílková[1,‡], Cyril Bařinka[2] and David Staněk[1,§]

ABSTRACT

SART3 is a multifunctional protein that acts in several steps of gene expression, including assembly and recycling of the spliceosomal U4/U6 small nuclear ribonucleoprotein particle (snRNP). In this work, we provide evidence that SART3 associates via its N-terminal HAT domain with the 12S U2 snRNP. Further analysis showed that SART3 associates with the post-splicing complex containing U2 and U5 snRNP components. In addition, we observed an interaction between SART3 and the RNA helicase DHX15, which disassembles post-splicing complexes. Based on our data, we propose a model that SART3 associates via its N-terminal HAT domain with the post-splicing complex, where it interacts with U6 snRNA to protect it and to initiate U6 snRNA recycling before a next round of splicing.

KEY WORDS: Splicing, Recycling, U6 snRNA, U2 snRNP

INTRODUCTION

SART3 is a multifunctional protein involved in several steps of gene expression. This protein was first identified in a search to find the U6 small nuclear RNA (snRNA)-capping enzyme as a 110-kDa RNA-interacting protein and named p110^{nrb} (Gu et al., 1998). At the same time, SART3-derived peptides were shown to represent tumor epitopes inducing cytotoxic T cells against adenocarcinomas and squamous cell carcinoma, which gave the protein its official name (Yang et al., 1999). In 2002, two independent reports showed that SART3 is a novel HIV-1 Tat-interacting partner that enhances Tat transactivation activity and a U6 snRNA-interacting protein that promotes reassembly of U4/U6 small nuclear ribonucleoprotein particles (snRNPs) after splicing (Bell et al., 2002; Liu et al., 2002). SART3 was further found in the 7SK snRNP, where it interacts with the methyltransferase MEPCE, which methylates the γ phosphate at the 5′ end of 7SK and U6 snRNAs (Jeronimo et al., 2007; Yang et al., 2019). It was suggested that SART3 can influence 7SK composition and thus indirectly the activity of the P-TEFb complex (Liu et al., 2021). The diverse roles of SART3 in gene expression are thoroughly reviewed in Whitmill et al. (2016).

The function of SART3 described in the most detail is its role in the biogenesis and recycling of snRNPs, which are basic and essential building blocks of the spliceosome. The U4/U6 snRNP associates with the U5 snRNP and together enter the splicing reaction as a pre-assembled U4/U6•U5 tri-snRNP. During splicing, the extensive base-pairing between U4 and U6 is disrupted, and U6 establishes new interactions with pre-mRNA and U2 snRNA, and forms the catalytic center of the spliceosome. After splicing, U2, U5 and U6 snRNAs stay bound to the lariat and are released by RNA helicase DHX15 (called Prp43 in *Saccharomyces cerevisiae*) (Arenas and Abelson, 1997; Martin et al., 2002; Zhang et al., 2019). Yeast Prp43 acts in a complex with two co-factors, Ntr1 and Ntr2, where Ntr1 stimulates Prp43 helicase activity and together they disassemble the post-splicing complex (Fourmann et al., 2013; Tanaka et al., 2007; Tsai et al., 2005). A human ortholog of Ntr1 is the G-patch protein TFIP11, which stimulates DHX15-mediated post-splicing complex disassembly (Bohnsack et al., 2021; Yoshimoto et al., 2009).

Before the next round of splicing, U6 snRNA re-anneals with U4 snRNA and the splicing-competent tri-snRNP is reassembled. A yeast ortholog of SART3 called Prp24 associates with U6 snRNA and promotes base-pairing of U4/U6 snRNAs (Ghetti et al., 1995; Jandrositz and Guthrie, 1995; Montemayor et al., 2014, 2018; Rader and Guthrie, 2002; Raghunathan and Guthrie, 1998). Similarly, human SART3 interacts with the U6 and U4/U6 snRNPs, and re-anneals U4/U6 and U4atac/U6atac after splicing (Bell et al., 2002; Damianov et al., 2004; Medenbach et al., 2004). Recently, several non-coding RNAs interacting with SART3 were identified and suggested to modulate the SART3-mediated U4/U6 annealing (De Troyer et al., 2020; El Fatimy et al., 2022). SART3 localizes to the nucleoplasm and nuclear Cajal bodies (Liu et al., 2002; Staněk et al., 2003), and rapidly shuttles between these nuclear compartments (Dundr et al., 2004; Novotný et al., 2011). A more detailed analysis by fluorescence resonance energy transfer revealed that a nucleoplasmic pool of SART3 interacts mainly with the U6 snRNP, whereas SART3 in Cajal bodies associates with the U4/U6 snRNP (Staněk and Neugebauer, 2004). It was proposed that U4/U6 annealing occurs in Cajal bodies, which makes the process more efficient (Klingauf et al., 2006; Novotný et al., 2011). In addition to its U4/U6 snRNA-annealing function, SART3 was suggested as a proofreading factor that sequesters incomplete snRNPs in Cajal bodies (Novotný et al., 2015).

SART3 is an acidic, 963 amino acid-long protein which contains several distinct domains. At the N-terminus, there is an unstructured glutamic acid-rich region, called the E domain, that interacts with coilin (Novotný et al., 2015). The E-domain is followed by 12 half-a-tetratricopeptide (HAT) repeats organized into two subdomains. The concave surface of the HAT-C subdomain allows the formation of a homodimer, whereas the opposite convex surface binds the USP4 or USP15 deubiquitinases, which remove ubiquitin from PRPF3 and PRPF31 and thus modulate interactions among snRNP proteins (Das et al., 2017; Park et al., 2016; Song et al., 2010; Zhang et al., 2016). The HAT domain is also responsible for the association with the U4/U6 snRNP-specific protein PRPF3 (Medenbach et al., 2004). The last helix of HAT12 is extended and links the HAT region to a bipartite nuclear localization sequence (NLS). Two RNA-recognition motifs (RRMs) span the C-terminal part of SART3 and bind U6 snRNA. The structure of RRMs bound to U6

[1]Department of RNA Biology, Institute of Molecular Genetics, Czech Academy of Sciences, 142 20 Prague, Czech Republic. [2]Laboratory of Structural Biology, Institute of Biotechnology, Czech Academy of Sciences, 252 50 Prague, Czech Republic.
*Present address: DIANA Biotechnologies, Nad Safinou II 366, 252 50 Vestec, Czech Republic.
‡These authors contributed equally to this work

§Author for correspondence (stanek@img.cas.cz)

D.S., 0000-0002-5865-175X

Handling Editor: Maria Carmo-Fonseca
Received 27 June 2022; Accepted 10 December 2022

Journal of Cell Science (2023) 136, jcs260380. doi:10.1242/jcs.260380

snRNA was solved for yeast Prp24 and revealed an interesting architecture of two interlocked rings, which involves U6 snRNA and four Prp24 RRMs (Montemayor et al., 2014). Human SART3 contains only two RRMs and the interaction with U6 snRNA might be achieved via SART3 dimerization. Interestingly, the RRM domains of SART3 and Prp24 binds the highly conserved nucleotides ACAGAG of U6 snRNA, which are involved in splicing catalysis (Bell et al., 2002; Liu et al., 2015; Medenbach et al., 2004; Montemayor et al., 2014). The last ten amino acids at the C-terminus are conserved between various species and bind the U6-specific ring composed of seven LSm proteins, LSm2–8 (Montemayor et al., 2018; Rader and Guthrie, 2002).

In this report, we studied an unexpected interaction between SART3 and the U2 snRNP. We combined immunoprecipitation with gradient centrifugation to analyze U2-containing complexes that associate with the SART3 N-terminal domain. We provide evidence that the N-terminal half of SART3 interacts with the 12S U2 snRNP particle and DHX15 helicase. Taken together, our data suggest that SART3 is tethered via its HAT domain to the post-splicing complex to interact with U6 snRNA and initiate its recycling.

RESULTS

Some of the previous studies indicated a weak interaction of SART3 with U2 snRNA, which increased after deletion of the C-terminal part containing both RRMs (Medenbach et al., 2004; Novotný et al., 2015). To confirm these results, we first prepared several SART3 deletion variants tagged with enhanced green fluorescence protein (GFP) (Fig. 1A). In addition to wild-type SART3 (WT-SART3), we expressed a variant lacking the twelfth HAT domain mediating SART3 dimerization (ΔCC-SART3) (Huang et al., 2018), SART3 without the N-terminal E-domain that is important for association with coilin (ΔE-SART3) and mutants lacking either the whole HAT domain (C-SART3) or the C-terminus containing the RRMs and the conserved C-terminal tail (N-SART3), which were characterized previously (Novotný et al., 2015; Staněk et al., 2003). We transiently transfected these constructs into HeLa cells and monitored their localization and expression (Fig. S1). Consistent with previous observations, the SART3 construct lacking the HAT domain (C-SART3) failed to accumulate in Cajal bodies and localized to the nucleoplasm and nucleoli, which is likely non-specific because GFP–NLS exhibits similar localization (Staněk et al., 2003). Deletion of the dimerization HAT12 domain (ΔCC-SART3) also reduced Cajal body targeting (Fig. S1A,B). WT SART3–GFP and N-SART3–GFP were expressed better than the other variants, but this difference was partially diminished after immunoprecipitation and all constructs were immunoprecipitated to a similar extent (Fig. S1C). Finally, we monitored the effect of SART3 construct expression on splicing and did not observe any significant changes in splicing efficiency of seven selected genes (Fig. S1D).

To monitor SART3 association with U2 snRNA, we transiently expressed all SART3–GFP variants, immunoprecipitated them with anti-GFP antibodies and analyzed the co-purified snRNAs by silver staining in a polyacrylamide gel and reverse transcription followed by quantitative PCR (RT-qPCR) (Fig. 1B,C). The interaction of WT SART3–GFP with U2 snRNA was relatively weak compared to its interaction with U4 and U6 snRNAs (Fig. 1B), but increased 5-fold when the C-terminus of SART3 was missing (N-SART3; Fig. 1B, C). We did not detect any U2 binding after the deletion of the entire HAT (C-SART3) or HAT12 (ΔCC-SART3) domains (Fig. 1B), indicating that the HAT domain is necessary for U2 snRNA association and that the interaction is either mediated by HAT12 or requires the formation of SART3 homodimers. To probe whether SART3 interacts with naked U2 snRNA or the U2 snRNP, we repeated the pulldown and monitored co-precipitation of the U2-specific protein SNRPA1 (U2A′) (Fig. 1D). A strong association between N-SART3–GFP and SNRPA1 indicated that the HAT domain of SART3 interacts with the U2 snRNP. Co-precipitation of USP15, which specifically interacts with the HAT domain, served as a positive control for SART3 pulldowns. To confirm the SART3–U2 interaction, we immunoprecipitated endogenous SNRPA1 and detected co-precipitated endogenous SART3 (Fig. 1E). We concluded that SART3 associates with the U2 snRNP primarily via the HAT domain.

The U2 snRNP localizes to Cajal bodies, a nuclear structure scaffolded by the protein coilin (Carmo-Fonseca et al., 1991; Machyna et al., 2015; Novotný et al., 2015). In our previous study, we observed a positive correlation between SART3 interaction with U2 snRNA and its interaction with coilin (Novotný et al., 2015). We therefore investigated whether SART3 associates with the U2 snRNP indirectly via coilin. We expressed WT SART3–GFP and N-SART3–GFP in coilin knockout (KO) HeLa cells (Basello et al., 2022). Coilin and SNRPA1 were co-precipitated with N-SART3–GFP in parental cells (wt), whereas only SNRPA1 co-purified with N-SART3–GFP in cells lacking coilin (KO), which indicates that the SART3–U2 interaction is coilin independent (Fig. 2A).

U2 snRNP maturation proceeds through several steps producing specific intermediates. The first 12S particle contains the core U2 snRNP (snRNA and Sm proteins) and SNRPA1 and SNRPB2 (U2B″) proteins. The 12S particle associates with the SF3B complex to produce the 15S particle. Finally, the trimeric SF3A complex joins and the mature, splicing competent 17S U2 snRNP is formed (Kramer et al., 2005). To analyze which of the U2 particles associate with SART3, we immunoprecipitated WT SART3–GFP and N-SART3–GFP and analyzed the co-precipitation of SNRPB2, SF3B4, a component of the SF3B complex, and SF3A3, a subunit of the SF3A complex (Fig. 2B). Co-purification of N-SART3–GFP with SNRPA1 (Fig. 1D,E, Fig. 2A) and SNRPB2 (Fig. 2B) indicated that N-SART3 preferentially interacts with the 12S U2 particle and only weakly with the 15S particle, as indicated by weak co-precipitation of SF3B4 (Fig. 2B). To further probe the SART3 interaction with U2 components, we purified recombinant N-SART3 tagged with a combined Strep–FLAG–HALO tag (termed N-SART3–FLAG; Fig. S2A) and incubated the recombinant protein with cell lysates. Recombinant N-SART3–FLAG pulled down SNRPB2 but not SF3B4, which is consistent with the model that SART3 preferentially interacts with the 12S U2 snRNP (Fig. 2C). Finally, we transiently expressed N-SART3 tagged with the FLAG tag in HeLa cells and immunoprecipitated N-SART3–FLAG using the anti-FLAG antibody. We eluted complexes co-purified with N-SART3–FLAG with the FLAG peptide and analyzed them by ultracentrifugation in a glycerol gradient (Fig. 2D; Fig. S2B,C). The SNRPA1/SNRPB2-containing complex sedimented at 12S, confirming previous results and showing that N-SART3 associates with U2 snRNA in the form of the 12S particle.

The 12S U2 snRNP is formed during the biogenesis of the mature U2 particle or, alternatively, the 12S U2 snRNP is released after splicing when the U2 snRNP loses both the SF3A and SF3B complexes (Bessonov et al., 2008; Wahl et al., 2009; Zhang et al., 2019). To test, whether SART3 associates with newly assembled U2 particles, we utilized U2 snRNAs containing the MS2 loop, which we previously used to characterize proteins associated with

Journal of Cell Science (2023) 136, jcs260380. doi:10.1242/jcs.260380

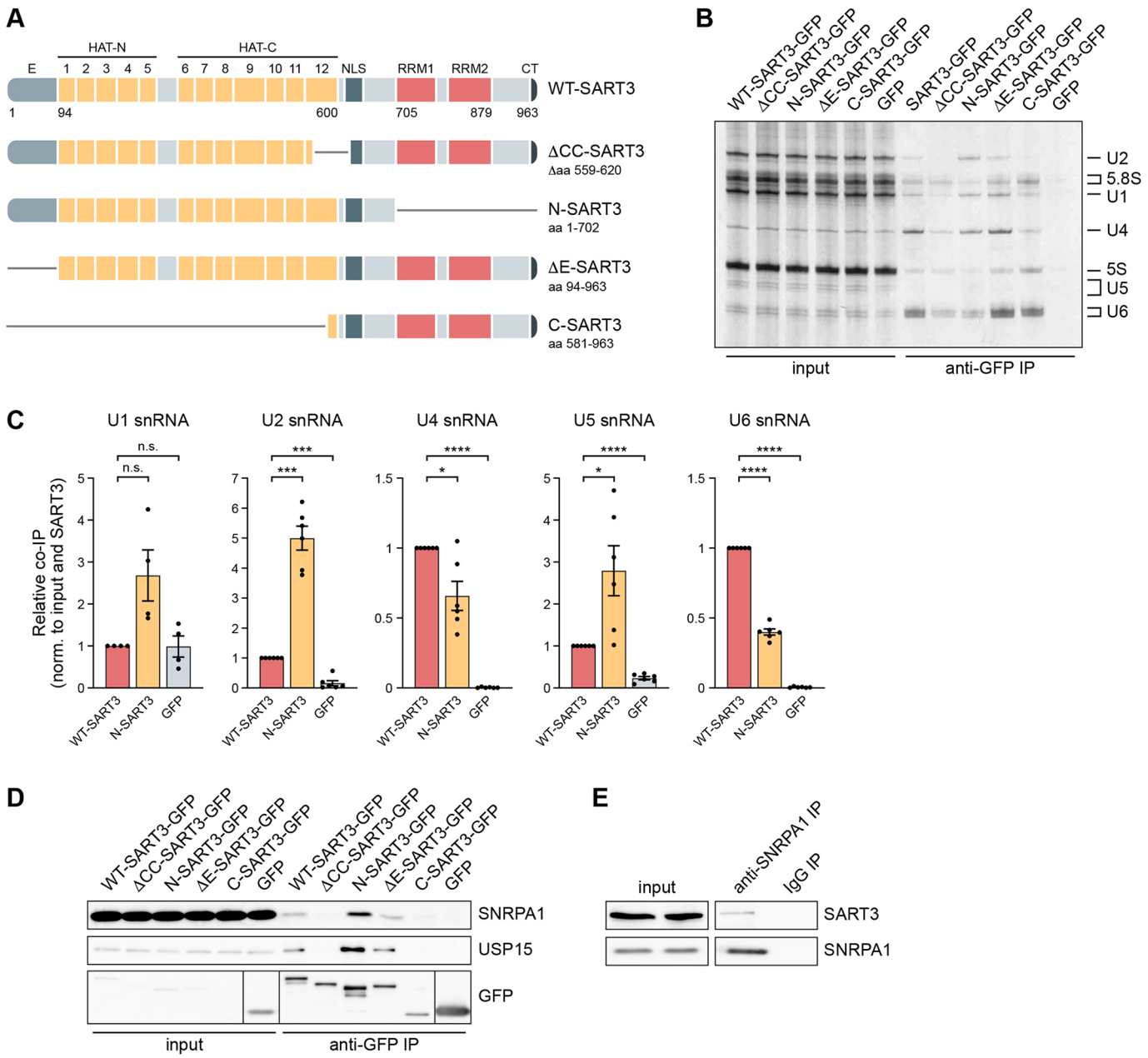

Fig. 1. The HAT domain of SART3 interacts with U2 snRNP. (A) A schematic representation of SART3 variants used in this study. (B,C) SART3–GFP constructs were transiently expressed in HeLa cells, immunoprecipitated with anti-GFP antibodies and the co-precipitated RNAs were resolved on urea polyacrylamide gels and silver stained (B), or quantified by RT-qPCR (C). Data show the mean±s.e.m. (n=4–6). n.s., not significant; *P<0.05; ***P<0.001; ****P<0.0001 (paired two-tailed Student's t-test). (D) SART3–GFP constructs were immunoprecipitated as before and the co-purified proteins were analyzed by western blotting. (E) Endogenous SNRPA1 was immunoprecipitated and the co-precipitation of endogenous SART3 was assayed by western blotting. Non-specific mouse IgG served as a negative control (IgG). Results shown are representative of at least two independent experiments.

truncated U2 snRNAs (Roithová et al., 2020, 2018) (Fig. 2E). U2-MS2 snRNA constructs interact with the MS2–YFP protein and can be immunoprecipitated by anti-GFP antibodies. Deletion of the 5′ half of U2 snRNA containing stem loops 1 and 2a/b does not block the interaction with SNRPA1 and SNRPB2 but prevents association with the SF3A and SF3B proteins (Fig. 2E) (Roithová et al., 2018), and thus mimics newly formed 12S complexes. WT U2-MS2 interacts with all tested U2-specific proteins, but we did not find any association with the U5-specific proteins PRPF8 and PRPF6. This finding indicates that WT U2-MS2 snRNA is not incorporated in the spliceosome either due to the inhibitory effect of the MS2 loop or because, within 24 h after transfection, only a small number of U2-MS2 snRNAs reaches the final maturation and participates in splicing. Neither the WT U2-MS2 snRNA nor the truncated U2-MS2 snRNA pulled down SART3, which strongly suggests that SART3 does not associate with newly formed 12S U2 particles during their biogenesis.

We therefore assumed that SART3 interacts with the post-splicing U2 snRNP. We further hypothesized that under physiological conditions, SART3 is able to associate with post-splicing complexes that contain incomplete U2 snRNPs. According to our model, SART3 binds U6 snRNA and they leave the

Journal of Cell Science (2023) 136, jcs260380. doi:10.1242/jcs.260380

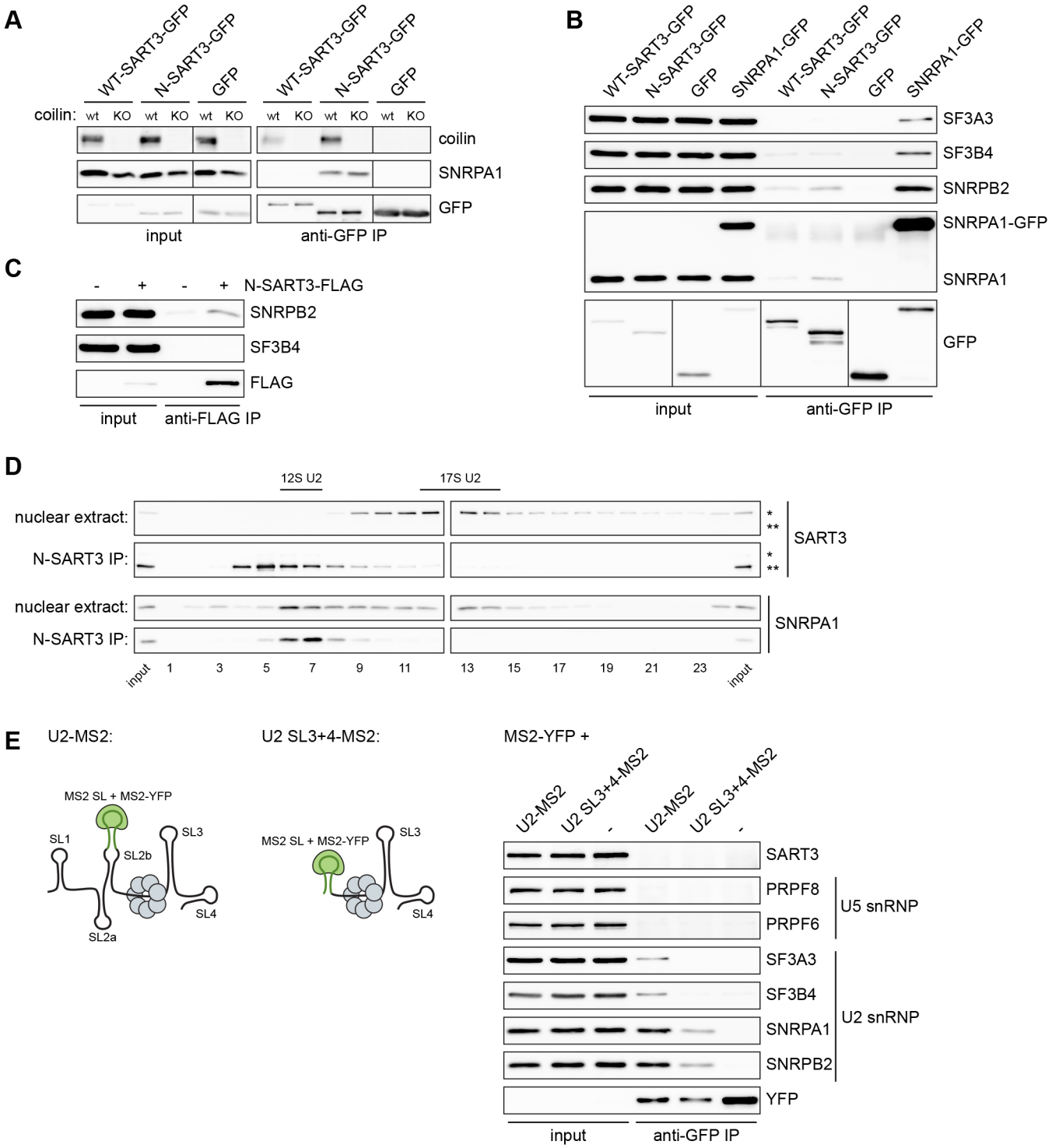

Fig. 2. See next page for legend.

post-splicing complex together. However, the deletion of the C-terminal region prevents U6 snRNA binding, which affects correct SART3 release from the post-splicing complex and results in the observed stronger association with the post-splicing U2 snRNP (Figs 1 and 2). To test this hypothesis, we decided to investigate whether SART3-U2 particles also contain splicing and post-splicing factors. We transiently expressed WT SART3 and N-SART3 tagged with GFP containing a TEV cleavage site. In the first step, SART3-associated complexes were immunoprecipitated by anti-GFP antibodies (Fig. 3A). The bound complexes were then released by the treatment with the TEV protease and subjected to a second immunoprecipitation with the anti-SNRPA1 antibody (Fig. 3B). The complexes isolated by single or double immunoprecipitation contained the key splicing protein PRPF8, a component of the NineTeen Complex (NTC), PRPF19 and the RNA helicase DHX15 (Fig. 3A,B). Analysis of snRNA components revealed that

Journal of Cell Science

Journal of Cell Science (2023) 136, jcs260380. doi:10.1242/jcs.260380

Fig. 2. SART3 interacts with 12S U2 snRNP. (A) SART3–GFP constructs were transiently expressed in parental HeLa (wt) or Hela^{coilinKO} (KO) cells and immunoprecipitated with anti-GFP antibodies, and the co-precipitation of coilin and SNRPA1 was assayed by western blotting. (B) SART3–GFP constructs were transiently expressed in parental HeLa cells and the co-purification of SNRPB2 (a protein found in all 12S, 15S and 17S particles), SF3B4 (a protein found in 15S and 17S particles) and SF3A3 (a marker of 17S particle) was monitored by western blotting. Immunoprecipitation of SNRPA1–GFP served as a positive control. (C) Recombinant N-SART3–FLAG was incubated with cell lysates and precipitated by the anti-FLAG antibody, and the co-purified proteins were analyzed by western blotting. (D) N-SART3–FLAG was transiently expressed in HeLa cells and immunoprecipitated with the anti-FLAG antibody. Co-precipitated complexes were eluted by the FLAG peptide and resolved by ultracentrifugation in a 10–30% glycerol gradient. Proteins were isolated from individual fractions and SNRPA1 and SART3 were detected by western blotting. The position of endogenous SART3 is indicated by an asterisk (*), and that of N-SART3–FLAG by two asterisks (**). The position of U2 snRNP particles in the gradient was determined by the analysis of snRNP complexes in nuclear extracts performed in parallel (see Fig. S2B). (E) U2-MS2 and U2_SL3+4-MS2 snRNAs were transiently expressed in HeLa cells together with the MS2–YFP protein and immunoprecipitated with anti-GFP antibodies (cross-reacting with YFP). The co-precipitated proteins were analyzed by western blotting (right). Cells transfected only with MS2–YFP (–) served as a negative control. In the schematic (left), the green blob represents MS2–YFP and grey balls represent the Sm proteins. The positions of individual stem loops (SL1–4) as well as the MS2 loop in U2 snRNA are indicated. Results shown are representative of at least two independent experiments.

N-SART3–U2 complexes contained more U5 snRNA and less U6 snRNA than WT SART3–U2 double pulldowns (Fig. 3C; Fig. S3A), which indicates that N-SART3, which lacks the U6-interacting RRMs, is unable to leave with U6 snRNA and stays artificially bound in the post-splicing complex with U2 and/or U5 snRNAs. To further analyze N-SART3–U2 complexes, we immunoprecipitated transiently expressed N-SART3–FLAG from cell lysates, eluted bound complexes with the FLAG peptide and analyzed them by ultracentrifugation in glycerol gradients (Fig. 3D; Fig. S3B). Only a small amount of DHX15 co-sedimented with the N-SART3 (fractions 2–4). In the same fractions, we also detected the deubiquitinase USP15, a known interactor of SART3 (Fig. 3D), and SNRPB2 (Fig. S3C).

To further investigate interactions between SART3 and post-splicing factors, we analyzed the direct interaction between N-SART3 and the U2 proteins SNRPA1 and SNRPB2, and the RNA helicase DHX15. These proteins and the SART3 interaction domain of PRPF3, used as a positive control (Medenbach et al., 2004), were *in vitro* translated using a coupled transcription/translation kit and pulled down with recombinant N-SART3–FLAG (Fig. 4A). SNRPA1 was very poorly expressed and we could not draw a conclusion about the SNRPA1–SART3 interaction. Pulldown of SNRPB2 with recombinant N-SART3–FLAG was weak and similar to the negative control (3×FLAG). Finally, we observed a weak interaction between SART3 and DHX15. Furthermore, SART3 precipitated the N-terminal part of DHX15 [amino acids (aa) 1–320], which includes the N-terminal disordered domain and the ATPase domain (UniProt ID: O43143). The experiment with the C-terminal part of DHX15 (aa 288–795) was inconclusive because this protein associated strongly with the 3×FLAG peptide. We further tested whether the interaction of SART3 or N-SART3 with post-splicing components is dependent on RNA (Fig. 4B). Although the interaction with U2 snRNP-specific proteins was RNase sensitive, pulldown of DHX15 was largely RNA independent, which is consistent with the direct protein–protein interaction between N-SART3 and DHX15. Consistently, N-SART3–GFP co-precipitation of U2-specific proteins was reduced upon DHX15 knockdown (Fig. 4C). Taken together, these data indicate that SART3 is attracted to the post-splicing complex via interaction with DHX15.

Dismantling of the post-splicing complex by DHX15 is activated by the G-patch protein TFIP11 (Bohnsack et al., 2021; Yoshimoto et al., 2009). To test whether TFIP11 plays any role in SART3 association with the post-splicing complex, we probed an interaction of SART3 and N-SART3 with TFIP11. We did not detect any association between SART3 or N-SART3 and TFIP11, but downregulation of TFIP11 reduced the interaction of WT SART3–GFP and N-SART3–GFP with U2-specific SNRPA1 and DHX15 (Fig. 4D). Similarly, association of endogenous SART3 and SNRPA1 was lost after knockdown of TFIP11 (Fig. 4E). These data suggest that TFIP11 activity is necessary for SART3 interaction with the post-splicing complex. Surprisingly, SART3 downregulation also reduced the interaction of TFIP11 with SNRPA1 (Fig. 4E). However, these effects might not be direct and could reflect global changes in the splicing machinery induced by the reduction of TFIP11 and SART3 (Duchemin et al., 2021; Trede et al., 2007).

DISCUSSION

SART3 is a known spliceosome recycling factor that interacts with U6 snRNA and regenerates U4/U6 snRNPs after splicing. Here, we mapped the association of SART3 with another splicing component, the U2 snRNP. We showed that the N-terminal half of SART3 containing the HAT repeats interacts with the 12S U2 snRNP. Our data further indicate that SART3 does not interact with newly formed particles during their biogenesis but rather with post-splicing U2 snRNP. Consistently, immunoprecipitated SART3–U2 complexes contain the splicing factors PRPF8 and PRPF19, which were found together in a post-splicing particle (Klimešová et al., 2021; Makarov et al., 2002), and the RNA helicase DHX15, which disassembles the post-splicing complex (Zhang et al., 2019). We further provide evidence that SART3 directly interacts with DHX15 and downregulation of DHX15 reduced SART3 association with the U2 snRNP (Fig. 4). To get further insight into the role of DHX15 in SART3 interaction with the post-splicing complexes, we probed TFIP11, the protein that activates DHX15 function in post-splicing complex disassembly (Bohnsack et al., 2021; Yoshimoto et al., 2009). We did not find any interaction between SART3 and TFIP11, but downregulation of TFIP11 prevented binding of N-SART3 to the U2 snRNP, which we consider to be a marker of N-SART3 interaction with the post-splicing complex (Fig. 4). However, TFIP11 knockdown also affects tri-snRNP formation and induces global changes in RNA splicing (Duchemin et al., 2021). Therefore, we cannot exclude the possibility that the observed reduction of SART3–U2 snRNP association upon TFIP11 downregulation is caused by reduced tri-snRNP assembly and overall splicing activity. Despite this uncertainty, based on all our results, we conclude that DHX15 and its activity are important for SART3 binding to the post-splicing complex. We observed similar levels of DHX15 co-purified with WT SART3–GFP and N-SART3–GFP (Figs 3 and 4), which is in contrast to the U2 and U5 snRNP components strongly preferring N-SART3. These findings suggest that the SART3–DHX15 interaction is only transient and DHX15 is not a ubiquitous constituent of the post-splicing snRNPs. However, we found traces amount of DHX15 in the N-SART3–U2 12S complex (Fig. 3). It should be noted that DHX15 was also found in the 17S U2 particle and together with SART3 in a 35S tri-snRNP (Chen et al., 2017; Will et al., 2002).

Journal of Cell Science (2023) 136, jcs260380. doi:10.1242/jcs.260380

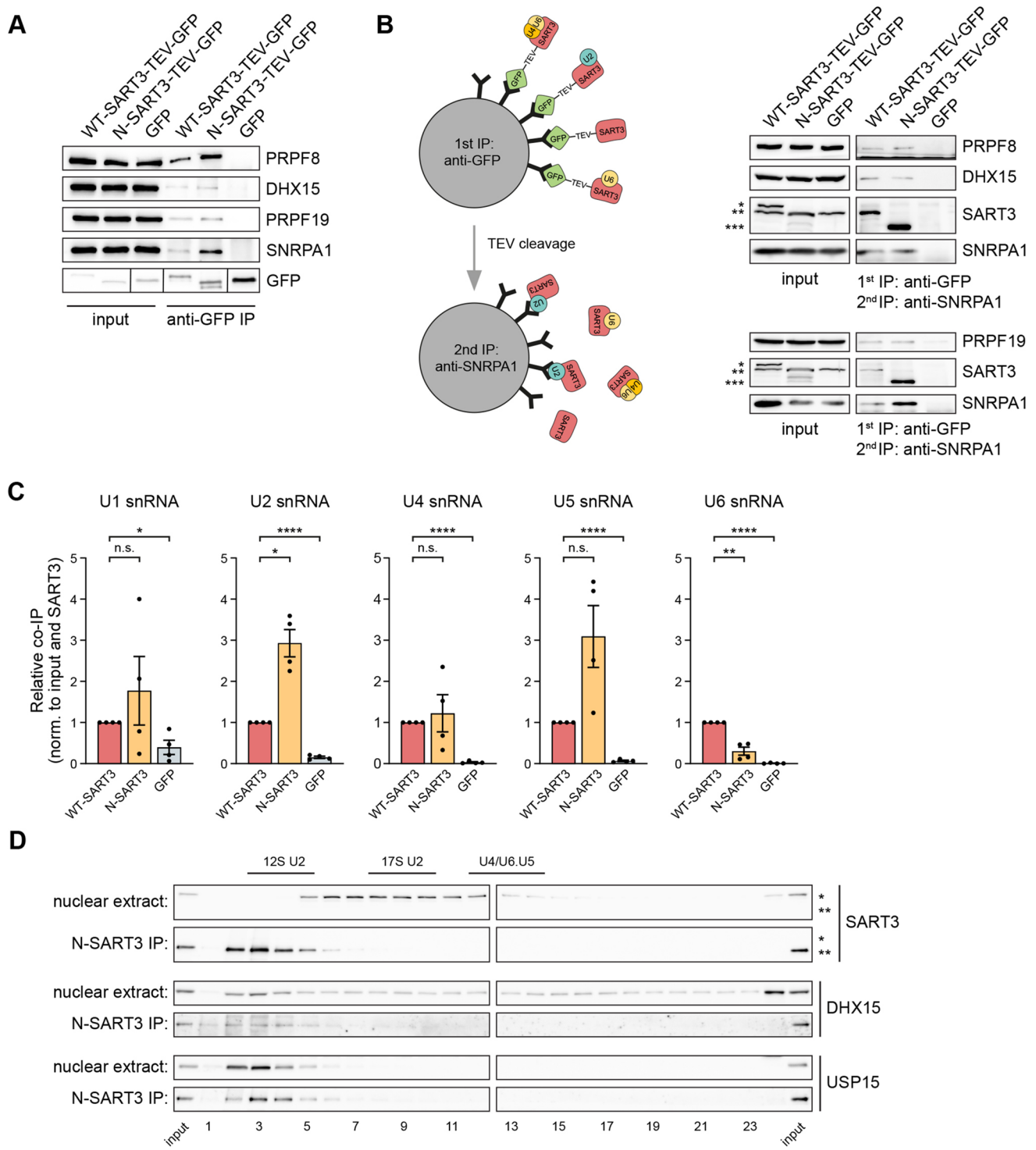

Fig. 3. SART3–U2 complexes contain additional splicing factors. (A) SART3–GFP constructs were transiently expressed in HeLa cells and immunoprecipitated with anti-GFP antibodies, and selected proteins from post-splicing complexes were detected by western blotting. (B) A schematic representation of double immunoprecipitation (IP). Proteins isolated by double immunoprecipitation with antibodies against GFP and SNRPA1 to pulldown N-SART3–TEV–GFP/SNRPA1 and SART3–TEV–GFP/SNRPA1 were analyzed by western blotting. Results of two independent experiments are shown. Asterisks (*) indicate SART3–TEV–GFP, two asterisks (**) indicate endogenous SART3, ectopically expressed SART3 after TEV cleavage and N-SART3–TEV–GFP, and three asterisks (***) mark N-SART3 after TEV cleavage. (C) snRNA co-purified by double immunoprecipitation were analyzed by RT-qPCR and double normalized to inputs and the signal in SART3–TEV–GFP/SNRPA1 pulldowns (see also Fig. S3A for alternative normalization to U2 snRNA signal). Data show the mean±s.e.m. (n=4). n.s., not significant; *P<0.05; **P<0.01; ****P<0.0001 (paired two-tailed Student's t-test). (D) N-SART3–FLAG was transiently expressed in HeLa cells and immunoprecipitated with the anti-FLAG antibody. Co-precipitated complexes were eluted by the FLAG peptide and resolved by ultracentrifugation in a 10–30% glycerol gradient. Proteins were isolated from individual fractions and SNRPA1 and SART3 were detected by western blotting. The position of endogenous SART3 is indicated by asterisks (*) and that of N-SART3–FLAG by two asterisks (**). The position of U2 snRNP particles in the gradient was determined by the analysis of snRNP complexes in nuclear extracts performed in parallel (see Fig. S3B). Results shown are representative of at least two independent experiments.

Journal of Cell Science (2023) 136, jcs260380. doi:10.1242/jcs.260380

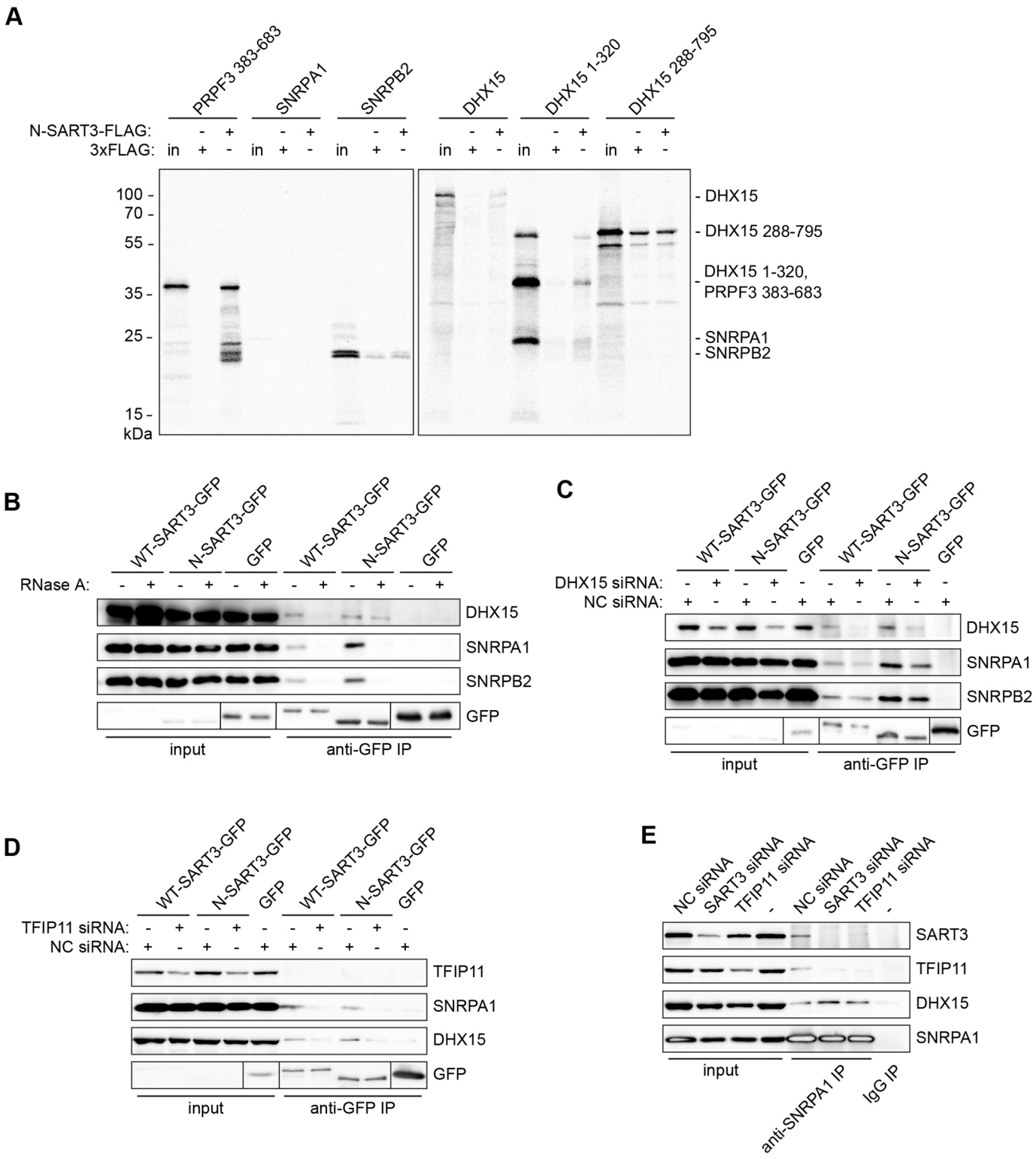

Fig. 4. DHX15 is important for SART3 association with the post-splicing complex. (A) Recombinant N-SART3–FLAG was incubated with *in vitro*-translated U2 snRNP-specific proteins (left panel) and DHX15 (right panel) labelled with ^{35}S and precipitated with anti-FLAG antibodies. We tested the interaction of N-SART3 with either full-length DHX15, the N-terminal region (aa 1–320) or the C-terminal region (aa 288–795). 3×FLAG served as a negative control and PRPF3 aa 383–683 as a positive control. 'in' indicates inputs. The immunoprecipitated proteins were detected by autoradiography. The extra bands above and below the DHX15 1–320 fragment are non-specific. (B) SART3–GFP constructs were transiently expressed in HeLa cells and before being immunoprecipitated with anti-GFP antibodies, cell lysates were treated with RNase A. Selected proteins from post-splicing complexes were detected by western blotting. (C,D) DHX15 (C) and TFIP11 (D) were downregulated by RNA interference and the interaction between SART3–GFP or N-SART3–GFP and selected proteins was monitored by immunoprecipitation followed by western blotting. (E) Immunoprecipitation of endogenous SNRPA1 after downregulation of SART3 or TFIP11. Co-precipitated proteins were analyzed by western blotting. Non-specific mouse IgG served as a negative control (IgG). Results shown are representative of at least two independent experiments.

Journal of Cell Science (2023) 136, jcs260380. doi:10.1242/jcs.260380

This indicates that DHX15 and SART3 can be present together in snRNPs, but the functional significance of DHX15 presence in various snRNP complexes is currently unclear.

The fate of snRNPs after splicing is not fully understood. The U5 snRNP leaves the post-splicing complex associated with the NTC complex as a 35S particle (Makarov et al., 2002; Makarova and Makarov, 2015). The chaperone TSSC4 that interacts with the post-splicing U5 snRNP and promotes recycling of the splicing-competent tri-snRNP has been recently described (Bergfort et al., 2022; Klimešová et al., 2021). Almost nothing is known about the recycling of the U2 snRNP, which needs to re-associate with the SF3B and SF3A complexes. This process might occur in Cajal bodies where defective SF3A components accumulate and where the recycling of U4/U6 was located as well (Nesic et al., 2004; Staněk et al., 2008). The presence of the USP15 deubiquitinase in N-SART3-associated 12S particles (Fig. 3) indicates that USP15 might assist in the recycling phase as well.

During splicing, snRNPs undergo substantial rearrangements and many snRNP-specific proteins are lost. It has been suggested that the binding of the U2-specific multi-component complexes SF3A and SF3B is significantly weakened during splicing and only the Sm proteins SNRPA1 and SNRPB2 stay bound to U2 snRNA (Bessonov et al., 2008; Wahl et al., 2009; Zhang et al., 2019). Similarly, U6 snRNA loses a ring of LSm2–8 proteins and it was suggested that U6 leaves the spliceosome as naked RNA (Didychuk et al., 2018; Fourmann et al., 2013). However, protein-free RNAs are unstable and all short non-coding nuclear RNAs exist together with proteins in the form of ribonucleoprotein particles. Based on our results we suggest that U6 snRNA is not released after splicing alone but bound by SART3. SART3 is attracted to the post-splicing complex via the interaction of its HAT domain with DHX15, then binds U6 snRNA, and SART3–U6 snRNA leave together. The C-terminal domain of SART3 then promotes interaction with LSm proteins and initiates U6 snRNP recycling. We have no evidence for the active role of SART3 in U6 snRNA release from the post-splicing complex. On the contrary, deletion of U6-interacting RRMs reduces the amount of U6 snRNA associated with the SART3–U2 particle (Fig. 3), which indicates that U6 is able to depart independently of SART3.

SART3 was described as a U4/U6 recycling factor, which associates with U6-specific LSm proteins and U6 snRNA and promotes U4/U6 snRNA annealing. Here we provide evidence that SART3 associates with the post-splicing complex and propose a model in which SART3 binds U6 snRNA after splicing and the U6 snRNA leaves with SART3 to initiate recycling phase for the next round of splicing. Consistently with this model, SART3–U6 complexes were found predominantly in the nucleoplasm; SART3 interacts with the U6 snRNA independently of LSm proteins both in humans and yeast and the SART3–U6–USIP-1 complex lacking Lsm proteins was identified in *Caenorhabditis elegans* (Bell et al., 2002; Montemayor et al., 2014; Ruegger et al., 2015; Staněk and Neugebauer, 2004). In addition, some, but not all, studies found SART3 associated with the lariat (Liu et al., 2015). SART3 is thus a key factor that guards U6 snRNA and promotes and controls its correct recycling between individual rounds of splicing.

MATERIALS AND METHODS

Cell culture

The HeLa cell line used in the study were received from Prof. Karla Neugebauer (Yale University, New Haven, CT, USA) and originated from the American Type Culture Collection HeLa-CCL-2 strain. They were further characterized in Hebert et al. (2002) as HeLa KN. HeLa cells were cultured in high-glucose (4.5 g/l) Dulbecco's modified Eagle's medium (DMEM, Sigma-Aldrich) supplemented with 10% fetal bovine serum (FBS, Gibco) and 1% penicillin/streptomycin (Gibco) and regularly tested for mycoplasma contamination. Suspension-adapted HEK293T17 cells (kindly provided by Ondrej Vanek, Charles University, Prague, Czech Republic) used for recombinant protein expression and purification were cultured in FreeStyle F17 Expression medium (Gibco) and grown in suspension. The HeLa coilin KO cell line is described in Basello et al. (2022).

Plasmids and transfection

The SART3, N-SART3, and C-SART3 sequences were cloned into pEGFP-N1 vector (Clontech) using BglII/EcoRI restriction sites, as described in Staněk et al. (2003). ΔE-SART3 was prepared by site-directed mutagenesis from full-length SART3-pEGFP-N1 (primer sequences are listed in Table S1). ΔCC-SART3-pEGFP-C3 was kindly provided by Caixia Guo (Beijing Institute of Genomics, Chinese Academy of Sciences) and characterized in Huang et al. (2018). The plasmids expressing SART3–TEV–GFP and N-SART3–TEV–GFP were obtained by insertion of the TEV cleavage site (5′-GAGAACCTGTACTTCCAGGGC-3′) using specific primers (Table S1). The plasmid expressing N-SART3–FLAG, which was used for immunoprecipitation and gradient ultracentrifugation, was obtained by subcloning of the N-SART3 sequence from the pEGFP-N1 vector to the pFLAG-C3 vector [pEGFP-C3 backbone (Clontech) where the GFP sequence was replaced with 3×FLAG]. The cloning was done by the Gibson assembly method (New England Biolabs) using the primers listed in Table S1. For the purposes of recombinant protein purification, N-SART3 was cloned into pDONR221 (Thermo Fisher Scientific) and subsequently into the pDEST_MM322 vector (Zessin et al., 2019) containing twin-Strep, FLAG and Halo tags using Gateway technology (Thermo Fisher Scientific) (primers used for PCR amplification of N-SART3 are listed in Table S1). The SNRPA1 and SNRPB2 coding sequences were cloned into a modified expression vector, pGL4-CMV (Addgene 100984), using XhoI/EcoRI restriction sites. The CMV promoter was removed and the Luciferase sequence was replaced by IRES sequence in the modified pGL4-CMV.

U2-MS2 constructs were described in Roithová et al. (2018). MS2–YFP plasmid was a kind gift from Yaron Shav-Tal (Bar-Ilan University, Ramat-Gan, Israel) and contains the NLS/NES nuclear shuttling domain from the HNRNPA1 protein. SNRPA1 was cloned into pEGFP-N1 using the BamHI/EcoRI restriction sites. All constructs were verified by DNA sequencing.

The plasmids were transiently transfected into HeLa cells using Lipofectamine 3000 Transfection Reagent (Thermo Fisher Scientific) according to the manufacturer's protocol. The cells were analyzed and processed 24 h after the transfection. HEK293T cells used for recombinant protein purification were transfected using linear polyethylenimine (PEI, Polysciences). N-SART3-pDEST_MM322 plasmid with the PEI was mixed with the cell suspension in FreeStyle F17 Expression medium (1 µg DNA per 0.5 ml of cell suspension). An equal amount of EX-CELL 293 serum-free medium (Sigma-Aldrich) was added after 4 h. The cells were cultured for 72 h.

RNA interference

The siRNA transfection was performed using Oligofectamine Transfection Reagent (Thermo Fisher Scientific) according to the manufacturer's instructions. siRNAs were transfected twice at a final concentration of 20 nM and incubated for 48 h after each transfection. Pre-annealed siRNA duplexes were obtained from Ambion: SART3, 5′-ACUGCUACGUGGAGUUUAAtt-3′ (Novotný et al., 2015); TFIP11 (s24424), 5′-CAAGGUAUCAUUAACCCAAtt-3′; DHX15 (s4029), 5′-GGUUAGACAUCAGUCCUUUtt-3′; and negative control no. 5 siRNA.

Antibodies

Immunoprecipitation was performed using antibodies against GFP (6 µg; provided by Pavel Tomancak, Max Planck Institute of Molecular Cell Biology and Genetics, Dresden, Germany), FLAG (2 µg, M2; or 2 µg, F7425; Sigma-Aldrich) and SNRPA1 (2 µg, ab128937, Abcam), and IgG antibody (1 µg, I5381, Sigma-Aldrich). For indirect fluorescent immunostaining, a primary antibody against coilin (1:1000, H-300, Santa

Journal of Cell Science (2023) 136, jcs260380. doi:10.1242/jcs.260380

Cruz Biotechnology) was used together with a secondary antibody conjugated with Alexa Fluor 555 (1:750, cat. no. A-21429, Thermo Fisher Scientific).

The following primary antibodies were used for western blotting: anti-GFP (1:500, B-2, Santa Cruz Biotechnology), anti-FLAG (1:1000, M2, Sigma-Aldrich), anti-SART3 (1:250, ab176822, Abcam), anti-USP15 (1:500, B-5, Santa Cruz Biotechnology), anti-SNRPA1 (1:4000, ab128937, Abcam), anti-SNRPB2 (1:2000, TA808139, Thermo Fisher Scientific; and 1:100, 57036, Progen), anti-SF3B4 (1:4000, ab183483; and 1:4000, ab104226; Abcam), anti-SF3A3 (1:4000, ab140605, Abcam), anti-PRPF8 (1:250, E-5, Santa Cruz Biotechnology), anti-PRPF6 (1:500, B-1, Santa Cruz Biotechnology), anti-PRPF19 (1:500, G-7, Santa Cruz Biotechnology), anti-DHX15 (1:300, E-6, Santa Cruz Biotechnology), anti-TFIP11 (1:500, C-7, Santa Cruz Biotechnology) and anti-coilin (1:2000, H-300, Santa Cruz Biotechnology). Secondary antibodies conjugated with horseradish peroxidase were used for western blotting detection (Jackson ImmunoResearch Laboratories).

Recombinant protein purification

HEK293T cells were centrifuged at 500 ***g*** and 4°C for 5 min and resuspended in lysis buffer (0.1 M Tris-HCl, pH 8.0, 10 mM NaCl, 5 mM KCl, 2 mM $MgCl_2$, 10% glycerol) supplemented with Complete Protease Inhibitor Cocktail (Roche) and benzonase. Cells were then sonicated by three 10 s pulses at 3 V, supplemented with 0.2% Nonidet P-40 (Sigma-Aldrich), and incubated on ice for 30 min. Cell lysates were centrifuged at 4500 ***g*** and 4°C for 15 min and then at 20,000 ***g*** and 4°C for 30 min. The recombinant protein tagged with twin-Strep was purified from the supernatant using Strep-Tactin Superflow resin (IBA Lifesciences) and eluted by elution buffer (50 mM Tris-HCl, pH 8.0, 150 mM NaCl, 10 mM KCl, 10% glycerol, 3 mM desthiobiotin).

Immunoprecipitation

Cells grown in 10 cm Petri dishes were harvested in ice-cold PBS, resuspended in NET2 buffer (50 mM Tris-HCl, pH 7.4, 150 mM NaCl, 0.05% Nonidet P-40) supplemented with Protease Inhibitor Cocktail Set III (Millipore) and RNasin ribonuclease inhibitor (Promega), and sonicated on ice by two 45 pulses (0.5 s at 40% of maximum energy). Cell lysates were centrifuged at 20,000 ***g*** and 4°C for 10 min. The supernatants were pre-cleaned by incubation with Protein G PLUS agarose beads (Santa Cruz Biotechnology) for 1 h at 4°C. Finally, the lysates were incubated overnight at 4°C with agarose beads with the pre-bound antibodies. 3% of the lysate was put aside before the immunoprecipitation step and used as an input sample.

For the immunoprecipitation after the RNase treatment, cells from 15 cm Petri dishes were used and divided equally into two samples after harvest. The lysates were prepared as described above. In the RNase-treated samples, addition of RNasin ribonuclease inhibitor (Promega) was omitted. After sonication, RNase A (Thermo Fisher Scientific) was added to the lysates (final concentration 0.1 mg/ml) and all samples were incubated at 37°C for 10 min. After the treatment, lysates were pre-cleaned and precipitated as described above.

For the pulldown of recombinant N-SART3–FLAG, the agarose beads were blocked by incubation with 1 mg/ml bovine serum albumin and 0.5 mg/ml sheared salmon sperm DNA (Ambion) in NET2 buffer (50 mM Tris-HCl, pH 7.4, 150 mM NaCl, 0.05% Nonidet P-40) for 1 h at 4°C before the binding of antibodies. The cell lysates were prepared as described above and 5 µg of recombinant protein was added and incubated with the lysate for 3 h at 4°C to allow formation of complexes between the recombinant and endogenous proteins.

For the two-step immunoprecipitation of SART3–U2 snRNP complexes, cells from two 15 cm Petri dishes were used per sample. The first step was done as described above. The beads with bound complexes were then washed with NET2 and treated with 8 µg of TEV protease (Sigma-Aldrich) in NET2 buffer overnight at 4°C. The released complexes were transferred to new beads and the second immunoprecipitation was performed.

After the immunoprecipitation, beads were washed with NET2 buffer and the proteins and RNA isolated. For protein analysis, the beads were directly mixed with SDS sample buffer (0.25 M Tris-HCl pH 6.8, 20% glycerol, 4% SDS, 2% β-mercaptoethanol, 0.02% bromophenol blue) and proteins resolved on a 10% polyacrylamide gel and detected by western blotting. The original western blot images are provided in Fig. S4. RNA was extracted using phenol/chloroform, dissolved in urea sample buffer (20 mM Tris-HCl pH 8.0, 8 M urea, 0.2% xylene blue), and then resolved on a 7 M urea denaturing polyacrylamide gel and silver stained. Alternatively, RNA was dissolved in nuclease-free water, reverse transcribed and analyzed by quantitative PCR.

In vitro protein pulldown assay

Proteins were *in vitro* transcribed and translated in the presence of ^{35}S-labeled methionine using TnT reticulocyte lysate system (Promega) according to the manufacturer's recommendation. The templates with the coding sequences of SNRPA1 and SNRPB2 were provided in the modified pGL4-CMV T7 expression vector (see above) and the templates with the coding sequences of PRPF3 aa 383–683, full-length DHX15, DHX15 aa 1–320 and DHX15 aa 288–795 were provided as T7 promotor PCR templates (primer sequences are listed in Table S1). 3% of the TnT reaction was used as input. For the pulldown assay, 25 µl of the TnT reaction was mixed with 5 µg of the recombinant N-SART3–FLAG protein or 3×FLAG peptide and incubated in NET2 buffer for 4 h at 4°C. The mixture of recombinant and TnT-produced proteins was pre-cleaned with Protein G PLUS agarose beads (Santa Cruz Biotechnology) for 1 h at 4°C and then incubated with agarose beads precoated with the primary anti-FLAG antibody overnight at 4°C. After the immunoprecipitation, the beads were washed with NET2 buffer, and the proteins were isolated, resolved on SDS polyacrylamide gels and detected by autoradiography.

RT-qPCR

For splicing efficiency analysis, cells were lysed and total RNA was isolated using TRIzol Reagent (Invitrogen) according to the manufacturer's protocol. The RNA pellet was resuspended in nuclease-free water, treated with Turbo DNase (Thermo Fisher Scientific) and precipitated, and 1 µg of the total RNA was then used for reverse transcription. For immunoprecipitated samples, 50% of immunoprecipitated or input RNA (regardless of the total concentration) was used per reaction. Reverse transcription was performed using SuperScript III (Thermo Fisher Scientific) and random hexamers. The cDNA was diluted 1:10 and analyzed by quantitative PCR using LightCycler 480 (Roche) and SYBR Green I reaction mix (Roche). The primer sequences are provided in Table S1. Splicing efficiency (ratio pre-mRNA/mRNA) was calculated as $[2^{Ct(mRNA) - Ct(pre\text{-}mRNA)}]$. The amount of co-precipitated snRNAs (IP) was normalized to snRNA levels in input samples. The ratio IP/input was calculated as $[2^{Ct(input) - Ct(IP)}]$.

Glycerol gradient ultracentrifugation

The complexes co-precipitated with N-SART3–FLAG were eluted from the beads by incubation with 25 µg of 3×FLAG peptide (Thermo Fisher Scientific) overnight at 4°C. Nuclear extracts were prepared using NE-PER Nuclear and Cytoplasmic Extraction Reagents (Thermo Fisher Scientific) according to the manufacturer's instructions. The samples were diluted to equal volume in gradient buffer (20 mM HEPES/KOH pH 8.0, 150 mM KCl, 1.5 mM $MgCl_2$) supplemented with Protease Inhibitor Cocktail Set III (Millipore), 0.5 mM phenylmethylsulfonyl fluoride and 0.5 mM dithiothreitol. Samples in the gradient buffer were loaded on a linear 10–30% glycerol gradient. Complexes were fractionated by centrifugation at 130,000 ***g*** (32,000 rpm) using a SW-40 Ti rotor (Beckman Coulter) for 17 h at 4°C (Fig. 2D; Fig. S2B,C) or at 79,000 ***g*** (25,000 rpm) for 16 h at 4°C (Fig. 3D; Fig. S3B,C). Individual fractions (500 µl each, 24 fractions in total) were collected and from every fraction, RNA and proteins were isolated using TRIzol Reagent (Invitrogen) according to the manufacturer's protocol.

Immunofluorescence and image acquisition

The cells were grown on coverslips and fixed with 4% paraformaldehyde/PIPES for 10 min at room temperature (RT). The fixed cells were treated with 0.2% Triton X-100 for 10 min at RT to achieve permeabilization,

blocked with 5% normal goat serum for 10 min at RT, and stained with primary antibodies diluted in PBS for 1 h at RT. After a PBS wash, the coverslips were stained with secondary antibodies for 1 h, washed again with PBS, and then mounted in Fluoromount-G (Southern Biotech) containing 4′,6-diamidino-2-phenylindole (DAPI).

Images were acquired using the DeltaVision microscope system (Applied Precision) coupled to the Olympus IX70 microscope equipped with a 60×/1.42 NA oil immersion objective, a CoolSNAP HQ2 camera (Photometrics; Princeton Instruments) and the acquisition software SoftWoRx (Applied Precision). Stacks of 20 *z*-sections with 200 nm *z*-steps were taken per sample and subjected to mathematical deconvolution using SoftWoRx software. Maximum intensity projections of deconvolved pictures are presented. For quantification of SART3–GFP variants in Cajal bodies, we took 25 *z*-sections with 25 nm *z*-steps. Cajal body localization analysis was performed in ImageJ Fiji software. Fluorescence intensities in Cajal bodies and in nuclei were measured from maximum intensity *z*-projections. The Cajal body:nucleoplasm fluorescence intensity ratios ($IF_{CB/nucleus}$) were determined from mean fluorescence intensity of a Cajal body or a nuclear region (IF_{CB} or $IF_{nucleus}$, respectively) and total fluorescence intensity or area ($area_{nucleus}$ indicates total area of the nucleoplasm) of all Cajal bodies per nucleus (total IF_{CB} or total $area_{CB}$, respectively) as:

$$IF_{CB/nucleus} = \frac{IF_{CB}}{\frac{IF_{nucleus} \times area_{nucleus} - total\ IF_{CB}}{area_{nucleus} - total\ area_{CB}}}.$$

Acknowledgements
We thank Caixia Guo, Pavel Tomancak and Yaron Shav-Tal for providing us with reagents. We also thank Helena Draberova for excellent technical assistance. The microscopy images were acquired at the Light Microscopy Core Facility, Institute of Molecular Genetics in Prague, Czech Republic, supported by Ministerstvo Školství, Mládeže a Tělovýchovy (LM2015062; CZ.02.1.01/0.0/0.0/16_013/0001775; CZ.2.16/3.1.00/21547).

Competing interests
The authors declare no competing or financial interests.

Author contributions
Conceptualization: K.K., H.P., D.S.; Methodology: K.K., H.P., C.B.; Validation: K.K., H.P.; Investigation: K.K., H.P.; Resources: K.K., H.P., C.B.; Writing - original draft: D.S.; Writing - review & editing: H.P., D.S.; Visualization: K.K., H.P.; Supervision: C.B., D.S.; Project administration: D.S.; Funding acquisition: D.S.

Funding
This work was supported by Grantová Agentura České Republiky (21-04132S), Ústav Molekulární Genetiky, Akademie Věd České Republiky (RVO68378050 and RVO68378050-KAV-NPUI) and Akademie Věd České Republiky (RVO86652036).

Data availability
All relevant data can be found within the article and its supplementary information.

Peer review history
The peer review history is available online at https://journals.biologists.com/jcs/article-lookup/doi/10.1242/jcs.260380.reviewer-comments.pdf

References
Arenas, J. E. and Abelson, J. N. (1997). Prp43: an RNA helicase-like factor involved in spliceosome disassembly. *Proc. Natl. Acad. Sci. USA* **94**, 11798-11802. doi:10.1073/pnas.94.22.11798

Basello, D. A., Matera, A. G. and Staněk, D. (2022). A point mutation in human Coilin prevents Cajal body formation. *J. Cell Sci.* **135**, jcs259587. doi:10.1242/jcs.259587

Bell, M., Schreiner, S., Damianov, A., Reddy, R. and Bindereif, A. (2002). p110, a novel human U6 snRNP protein and U4/U6 snRNP recycling factor. *EMBO J.* **21**, 2724-2735. doi:10.1093/emboj/21.11.2724

Bergfort, A., Hilal, T., Kuropka, B., Ilik, I. A., Weber, G., Aktaş, T., Freund, C. and Wahl, M. C. (2022). The intrinsically disordered TSSC4 protein acts as a helicase inhibitor, placeholder and multi-interaction coordinator during snRNP assembly and recycling. *Nucleic Acids Res.* **50**, 2938-2958. doi:10.1093/nar/gkac087

Bessonov, S., Anokhina, M., Will, C. L., Urlaub, H. and Lührmann, R. (2008). Isolation of an active step I spliceosome and composition of its RNP core. *Nature* **452**, 846-850. doi:10.1038/nature06842

Bohnsack, K. E., Ficner, R., Bohnsack, M. T. and Jonas, S. (2021). Regulation of DEAH-box RNA helicases by G-patch proteins. *Biol. Chem.* **402**, 561-579. doi:10.1515/hsz-2020-0338

Carmo-Fonseca, M., Pepperkok, R., Sproat, B. S., Ansorge, W., Swanson, M. S. and Lamond, A. I. (1991). In vivo detection of snRNP-rich organelles in the nuclei of mammalian cells. *EMBO J.* **10**, 1863-1873. doi:10.1002/j.1460-2075.1991.tb07712.x

Chen, Z., Gui, B., Zhang, Y., Xie, G., Li, W., Liu, S., Xu, B., Wu, C., He, L., Yang, J. et al. (2017). Identification of a 35S U4/U6.U5 tri-small nuclear ribonucleoprotein (tri-snRNP) complex intermediate in spliceosome assembly. *J. Biol. Chem.* **292**, 18113-18128. doi:10.1074/jbc.M117.797357

Damianov, A., Schreiner, S. and Bindereif, A. (2004). Recycling of the U12-type spliceosome requires p110, a component of the U6atac snRNP. *Mol. Cell. Biol.* **24**, 1700-1708. doi:10.1128/MCB.24.4.1700-1708.2004

Das, T., Park, J. K., Park, J., Kim, E., Rape, M., Kim, E. E. and Song, E. J. (2017). USP15 regulates dynamic protein-protein interactions of the spliceosome through deubiquitination of PRP31. *Nucleic Acids Res.* **45**, 4866-4880. doi:10.1093/nar/gkw1365

De Troyer, L., Zhao, P., Pastor, T., Baietti, M. F., Barra, J., Vendramin, R., Dok, R., Lechat, B., Najm, P., Van Haver, D. et al. (2020). Stress-induced lncRNA LASTR fosters cancer cell fitness by regulating the activity of the U4/U6 recycling factor SART3. *Nucleic Acids Res.* **48**, 2502-2517. doi:10.1093/nar/gkz1237

Didychuk, A. L., Butcher, S. E. and Brow, D. A. (2018). The life of U6 small nuclear RNA, from cradle to grave. *RNA* **24**, 437-460. doi:10.1261/rna.065136.117

Duchemin, A., O'Grady, T., Hanache, S., Mereau, A., Thiry, M., Wacheul, L., Michaux, C., Perpete, E., Hervouet, E., Peixoto, P. et al. (2021). DHX15-independent roles for TFIP11 in U6 snRNA modification, U4/U6.U5 tri-snRNP assembly and pre-mRNA splicing fidelity. *Nat. Commun.* **12**, 6648. doi:10.1038/s41467-021-26932-2

Dundr, M., Hebert, M. D., Karpova, T. S., Staněk, D., Xu, H., Shpargel, K. B., Meier, U. T., Neugebauer, K. M., Matera, A. G. and Misteli, T. (2004). In vivo kinetics of Cajal body components. *J. Cell Biol.* **164**, 831-842. doi:10.1083/jcb.200311121

El Fatimy, R., Zhang, Y., Deforzh, E., Ramadas, M., Saravanan, H., Wei, Z., Rabinovsky, R., Teplyuk, N. M., Uhlmann, E. J. and Krichevsky, A. M. (2022). A nuclear function for an oncogenic microRNA as a modulator of snRNA and splicing. *Mol. Cancer* **21**, 17. doi:10.1186/s12943-022-01494-z

Fourmann, J. B., Schmitzová, J., Christian, H., Urlaub, H., Ficner, R., Boon, K. L., Fabrizio, P. and Lührmann, R. (2013). Dissection of the factor requirements for spliceosome disassembly and the elucidation of its dissociation products using a purified splicing system. *Genes Dev.* **27**, 413-428. doi:10.1101/gad.207779.112

Ghetti, A., Company, M. and Abelson, J. (1995). Specificity of Prp24 binding to RNA: a role for Prp24 in the dynamic interaction of U4 and U6 snRNAs. *RNA* **1**, 132-145.

Gu, J., Shimba, S., Nomura, N. and Reddy, R. (1998). Isolation and characterization of a new 110 kDa human nuclear RNA- binding protein (p110nrb). *Biochim. Biophys. Acta* **1399**, 1-9. doi:10.1016/s0167-4781(98)00082-7

Hebert, M. D., Shpargel, K. B., Ospina, J. K., Tucker, K. E. and Matera, A. G. (2002). Coilin methylation regulates nuclear body formation. *Dev. Cell* **3**, 329-337. doi:10.1016/S1534-5807(02)00222-8

Huang, M., Zhou, B., Gong, J., Xing, L., Ma, X., Wang, F., Wu, W., Shen, H., Sun, C., Zhu, X. et al. (2018). RNA-splicing factor SART3 regulates translesion DNA synthesis. *Nucleic Acids Res.* **46**, 4560-4574. doi:10.1093/nar/gky220

Jandrositz, A. and Guthrie, C. (1995). Evidence for a Prp24 binding site in U6 snRNA and in a putative intermediate in the annealing of U6 and U4 snRNAs. *EMBO J.* **14**, 820-832. doi:10.1002/j.1460-2075.1995.tb07060.x

Jeronimo, C., Forget, D., Bouchard, A., Li, Q., Chua, G., Poitras, C., Thérien, C., Bergeron, D., Bourassa, S., Greenblatt, J. et al. (2007). Systematic analysis of the protein interaction network for the human transcription machinery reveals the identity of the 7SK capping enzyme. *Mol. Cell* **27**, 262-274. doi:10.1016/j.molcel.2007.06.027

Klimešová, K., Vojáčková, J., Radivojević, N., Vandermoere, F., Bertrand, E., Verheggen, C. and Staněk, D. (2021). TSSC4 is a component of U5 snRNP that promotes tri-snRNP formation. *Nat. Commun.* **12**, 3646. doi:10.1038/s41467-021-23934-y

Klingauf, M., Staněk, D. and Neugebauer, K. M. (2006). Enhancement of U4/U6 small nuclear ribonucleoprotein particle association in Cajal bodies predicted by mathematical modeling. *Mol. Biol. Cell* **17**, 4972-4981. doi:10.1091/mbc.e06-06-0513

Kramer, A., Ferfoglia, F., Huang, C. J., Mulhaupt, F., Nesic, D. and Tanackovic, G. (2005). Structure-function analysis of the U2 snRNP-associated splicing factor SF3a. *Biochem. Soc. Trans.* **33**, 439-442. doi:10.1042/BST0330439

Liu, Y., Li, J., Kim, B. O., Pace, B. S. and He, J. J. (2002). HIV-1 Tat protein-mediated transactivation of the HIV-1 long terminal repeat promoter is potentiated by a novel nuclear Tat-interacting protein of 110 kDa, Tip110. *J. Biol. Chem.* **277**, 23854-23863. doi:10.1074/jbc.M200773200

Liu, Y., Liu, J., Wang, Z. and He, J. J. (2015). Tip110 binding to U6 small nuclear RNA and its participation in pre-mRNA splicing. *Cell Biosci.* **5**, 40. doi:10.1186/s13578-015-0032-z

Liu, Y., Li, L., Timani, K., White, C. and He, J. J. (2021). Tip110 Expression Facilitates the Release of HEXIM1 and pTEFb from the 7SK Ribonucleoprotein Complex Involving Regulation of the Intracellular Redox Level. *Aging Dis.* **12**, 2113-2124. doi:10.14336/AD.2021.0528

Machyna, M., Neugebauer, K. M. and Staněk, D. (2015). Coilin: the first 25 years. *RNA Biol.* **12**, 590-596. doi:10.1080/15476286.2015.1034923

Makarova, O. V. and Makarov, E. M. (2015). The 35S U5 snRNP Is Generated from the Activated Spliceosome during In vitro Splicing. *PLoS One* **10**, e0128430. doi:10.1371/journal.pone.0128430

Makarov, E. M., Makarova, O. V., Urlaub, H., Gentzel, M., Will, C. L., Wilm, M. and Lührmann, R. (2002). Small nuclear ribonucleoprotein remodeling during catalytic activation of the spliceosome. *Science* **298**, 2205-2208. doi:10.1126/science.1077783

Martin, A., Schneider, S. and Schwer, B. (2002). Prp43 is an essential RNA-dependent ATPase required for release of lariat-intron from the spliceosome. *J. Biol. Chem.* **277**, 17743-17750. doi:10.1074/jbc.M200762200

Medenbach, J., Schreiner, S., Liu, S., Lührmann, R. and Bindereif, A. (2004). Human U4/U6 snRNP recycling factor p110: mutational analysis reveals the function of the tetratricopeptide repeat domain in recycling. *Mol. Cell. Biol.* **24**, 7392-7401. doi:10.1128/MCB.24.17.7392-7401.2004

Montemayor, E. J., Curran, E. C., Liao, H. H., Andrews, K. L., Treba, C. N., Butcher, S. E. and Brow, D. A. (2014). Core structure of the U6 small nuclear ribonucleoprotein at 1.7-A resolution. *Nat. Struct. Mol. Biol.* **21**, 544-551. doi:10.1038/nsmb.2832

Montemayor, E. J., Didychuk, A. L., Yake, A. D., Sidhu, G. K., Brow, D. A. and Butcher, S. E. (2018). Architecture of the U6 snRNP reveals specific recognition of 3'-end processed U6 snRNA. *Nat. Commun.* **9**, 1749. doi:10.1038/s41467-018-04145-4

Nesic, D., Tanackovic, G. and Krämer, A. (2004). A role for Cajal bodies in the final steps of U2 snRNP biogenesis. *J. Cell Sci.* **117**, 4423-4433. doi:10.1242/jcs.01308

Novotný, I., Blažíková, M., Staněk, D., Herman, P. and Malinsky, J. (2011). In vivo kinetics of U4/U6.U5 tri-snRNP formation in Cajal bodies. *Mol. Biol. Cell* **22**, 513-523. doi:10.1091/mbc.e10-07-0560

Novotný, I., Malinová, A., Stejskalová, E., Matějů, D., Klimešová, K., Roithová, A., Švéda, M., Knejzlík, Z. and Staněk, D. (2015). SART3-dependent accumulation of incomplete spliceosomal snRNPs in cajal bodies. *Cell Rep.* **10**, 429-440. doi:10.1016/j.celrep.2014.12.030

Park, J. K., Das, T., Song, E. J. and Kim, E. E. (2016). Structural basis for recruiting and shuttling of the spliceosomal deubiquitinase USP4 by SART3. *Nucleic Acids Res.* **44**, 5424-5437. doi:10.1093/nar/gkw218

Rader, S. D. and Guthrie, C. (2002). A conserved Lsm-Interaction Motif in Prp24 required for efficient U4/U6 di-snRNP Formation. *RNA* **8**, 1378-1392. doi:10.1017/S1355838202020010

Raghunathan, P. L. and Guthrie, C. (1998). A spliceosomal recycling factor that reanneals U4 and U6 small nuclear ribonucleoprotein particles. *Science* **279**, 857-860. doi:10.1126/science.279.5352.857

Roithová, A., Klimešová, K., Pánek, J., Will, C. L., Lührmann, R., Staněk, D. and Girard, C. (2018). The Sm-core mediates the retention of partially-assembled spliceosomal snRNPs in Cajal bodies until their full maturation. *Nucleic Acids Res.* **46**, 3774-3790. doi:10.1093/nar/gky070

Roithová, A., Feketová, Z., Vaňáčová, S. and Staněk, D. (2020). DIS3L2 and LSm proteins are involved in the surveillance of Sm ring-deficient snRNAs. *Nucleic Acids Res.* **48**, 6184-6197. doi:10.1093/nar/gkaa301

Ruegger, S., Miki, T. S., Hess, D. and Großhans, H. (2015). The ribonucleotidyl transferase USIP-1 acts with SART3 to promote U6 snRNA recycling. *Nucleic Acids Res.* **43**, 3344-3357. doi:10.1093/nar/gkv196

Song, E. J., Werner, S. L., Neubauer, J., Stegmeier, F., Aspden, J., Rio, D., Harper, J. W., Elledge, S. J., Kirschner, M. W. and Rape, M. (2010). The Prp19 complex and the Usp4Sart3 deubiquitinating enzyme control reversible ubiquitination at the spliceosome. *Genes Dev.* **24**, 1434-1447. doi:10.1101/gad.1925010

Staněk, D. and Neugebauer, K. M. (2004). Detection of snRNP assembly intermediates in Cajal bodies by fluorescence resonance energy transfer. *J. Cell Biol.* **166**, 1015-1025. doi:10.1083/jcb.200405160

Staněk, D., Rader, S. D., Klingauf, M. and Neugebauer, K. M. (2003). Targeting of U4/U6 small nuclear RNP assembly factor SART3/p110 to Cajal bodies. *J. Cell Biol.* **160**, 505-516. doi:10.1083/jcb.200210087

Staněk, D., Pridalova-Hnilicova, J., Novotny, I., Huranova, M., Blazikova, M., Wen, X., Sapra, A. K. and Neugebauer, K. M. (2008). Spliceosomal small nuclear ribonucleoprotein particles repeatedly cycle through Cajal bodies. *Mol. Biol. Cell* **19**, 2534-2543. doi:10.1091/mbc.e07-12-1259

Tanaka, N., Aronova, A. and Schwer, B. (2007). Ntr1 activates the Prp43 helicase to trigger release of lariat-intron from the spliceosome. *Genes Dev.* **21**, 2312-2325. doi:10.1101/gad.1580507

Trede, N. S., Medenbach, J., Damianov, A., Hung, L.-H., Weber, G. J., Paw, B. H., Zhou, Y., Hersey, C., Zapata, A., Keefe, M. et al. (2007). Network of coregulated spliceosome components revealed by zebrafish mutant in recycling factor p110. *Proc. Natl. Acad. Sci. USA* **104**, 6608-6613. doi:10.1073/pnas.0701919104

Tsai, R.-T., Fu, R.-H., Yeh, F.-L., Tseng, C.-K., Lin, Y.-C., Huang, Y.-H. and Cheng, S.-C. (2005). Spliceosome disassembly catalyzed by Prp43 and its associated components Ntr1 and Ntr2. *Genes Dev.* **19**, 2991-3003. doi:10.1101/gad.1377405

Wahl, M. C., Will, C. L. and Lührmann, R. (2009). The spliceosome: design principles of a dynamic RNP machine. *Cell* **136**, 701-718. doi:10.1016/j.cell.2009.02.009

Whitmill, A., Timani, K. A., Liu, Y. and He, J. J. (2016). Tip110: physical properties, primary structure, and biological functions. *Life Sci.* **149**, 79-95. doi:10.1016/j.lfs.2016.02.062

Will, C. L., Urlaub, H., Achsel, T., Gentzel, M., Wilm, M. and Lührmann, R. (2002). Characterization of novel SF3b and 17S U2 snRNP proteins, including a human Prp5p homologue and an SF3b DEAD-box protein. *EMBO J.* **21**, 4978-4988. doi:10.1093/emboj/cdf480

Yang, D., Nakao, M., Shichijo, S., Sasatomi, T., Takasu, H., Matsumoto, H., Mori, K., Hayashi, A., Yamana, H., Shirouzu, K. et al. (1999). Identification of a gene coding for a protein possessing shared tumor epitopes capable of inducing HLA-A24-restricted cytotoxic T lymphocytes in cancer patients. *Cancer Res.* **59**, 4056-4063.

Yang, Y., Eichhorn, C. D., Wang, Y., Cascio, D. and Feigon, J. (2019). Structural basis of 7SK RNA 5'-γ-phosphate methylation and retention by MePCE. *Nat. Chem. Biol.* **15**, 132-140. doi:10.1038/s41589-018-0188-z

Yoshimoto, R., Kataoka, N., Okawa, K. and Ohno, M. (2009). Isolation and characterization of post-splicing lariat-intron complexes. *Nucleic Acids Res.* **37**, 891-902. doi:10.1093/nar/gkn1002

Zessin, M., Kutil, Z., Meleshin, M., Nováková, Z., Ghazy, E., Kalbas, D., Marek, M., Romier, C., Sippl, W., Bařinka, C. et al. (2019). One-atom substitution enables direct and continuous monitoring of histone deacylase activity. *Biochemistry* **58**, 4777-4789. doi:10.1021/acs.biochem.9b00786

Zhang, Q., Harding, R., Hou, F., Dong, A., Walker, J. R., Bteich, J. and Tong, Y. (2016). Structural Basis of the Recruitment of Ubiquitin-specific Protease USP15 by Spliceosome Recycling Factor SART3. *J. Biol. Chem.* **291**, 17283-17292. doi:10.1074/jbc.M116.740787

Zhang, X., Zhan, X., Yan, C., Zhang, W., Liu, D., Lei, J. and Shi, Y. (2019). Structures of the human spliceosomes before and after release of the ligated exon. *Cell Res.* **29**, 274-285. doi:10.1038/s41422-019-0143-x

Figure S1

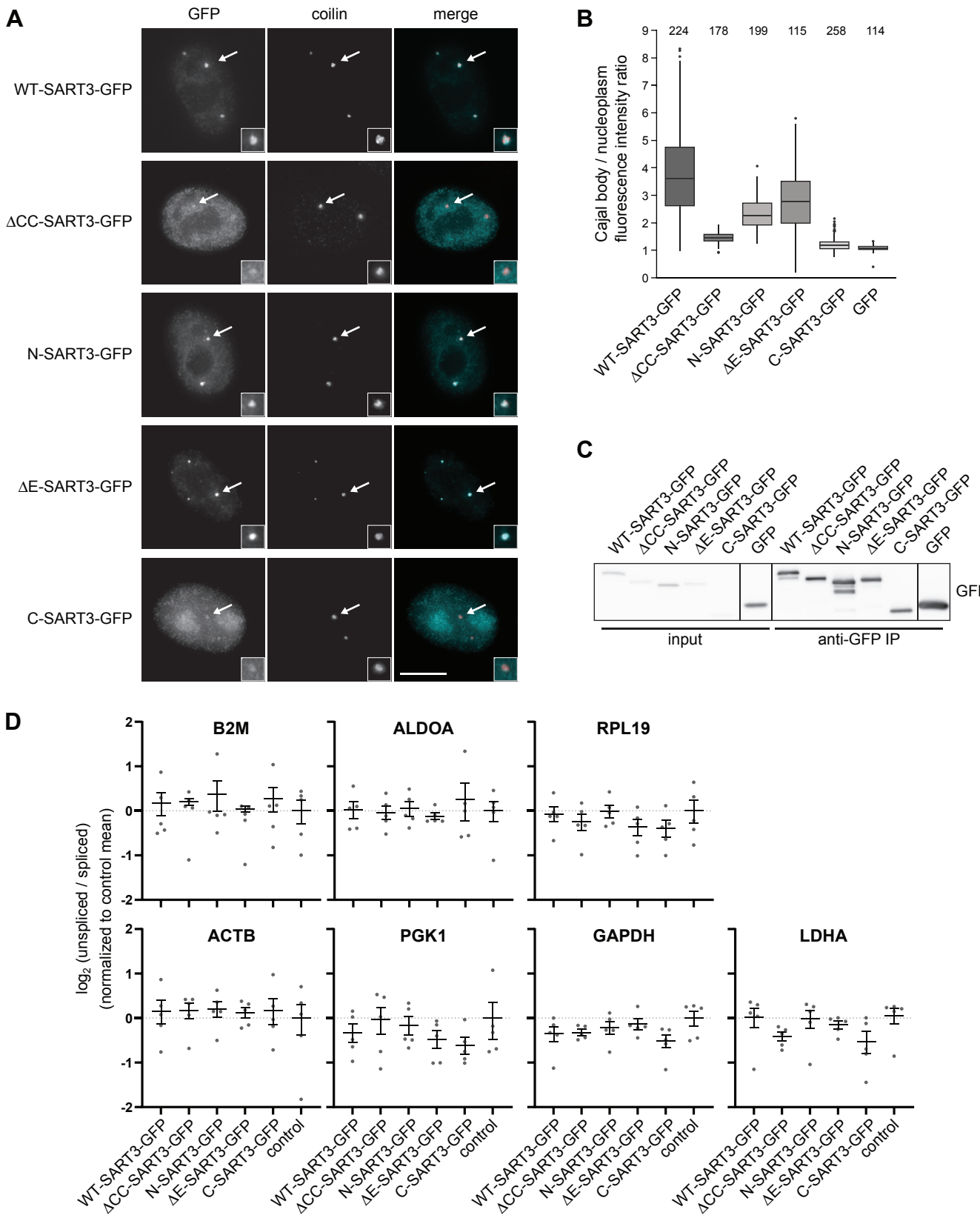

Fig. S1. **Localization and expression of SART3 variants.** (A) SART3-GFP constructs (see Fig. 1A) were transiently expressed in HeLa cells and their localization monitored by fluorescence microscopy (A). Coilin, a marker of Cajal bodies was visualized by indirect immunofluorescence. Cajal bodies marked by arrows were two-fold magni-fied and are shown in insets. In merged images, coilin is shown in red, GFP fluorescence in turquoise and the scale bar represents 10 µm. (B) Accumulation of SART3-GFP constructs in Cajal bodies was quantified by measuring GFP intensities in the Cajal body and the nucleoplasm. Number of Cajal bodies assayed is indicated above the graph. Statistical significance was tested by two-tailed, unpaired t-test. Changes are significant in all cases with $p<0.001$. (C) Expression level of SART3-GFP constructs in cell lysates and after immunoprecipitation with anti-GFP antibodies was monitored by western blotting using the mouse anti-GFP antibody. (D) SART3-GFP constructs were transiently expressed in HeLa cells and unspliced/spliced products of selected genes were monitored by reverse transcription followed by quantitative PCR. Mean and s.e.m. from five biological replicates are shown.

Journal of Cell Science • Supplementary information

Figure S2

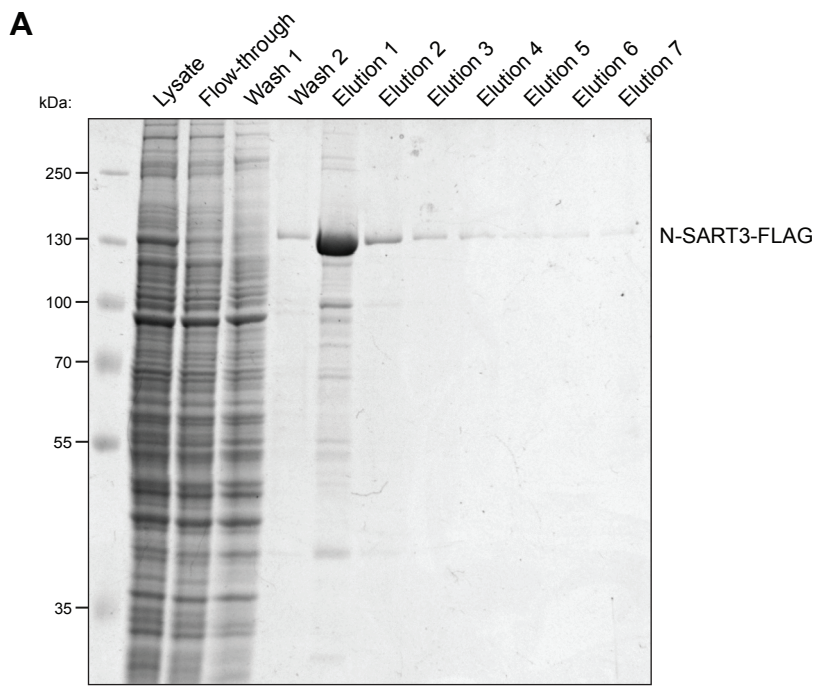

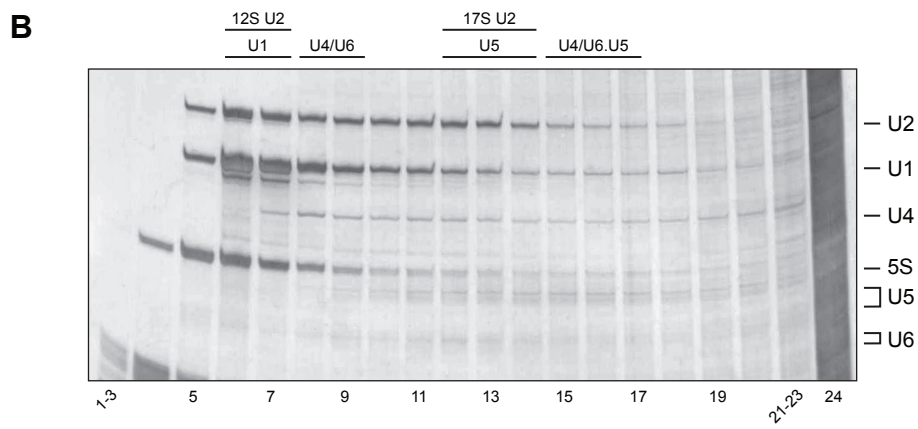

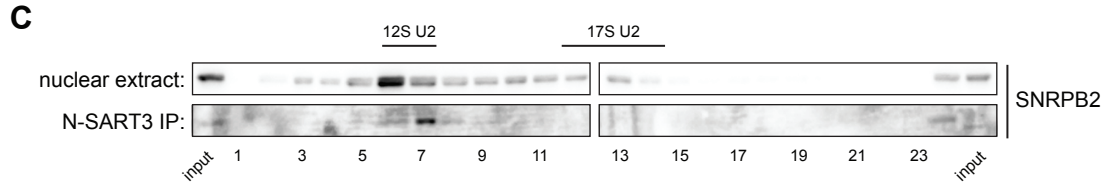

Fig. S2. Isolation of recombinant N-SART3 and monitoring distribution of snRNAs in glycerol gradient after ultracentrifugation. (A) A Coomassie blue stained polyacrylamide gel showing isolation of recombinant N-SART3- Strep-FLAG-HALO. (B) Nuclear extract was subjected to ultracentrifugation in 10-30% glycerol gradient, RNA from individual fractions isolated, resolved on denaturing UREA polyacrylamide gels and silver stained. Position of individual snRNP particles is indicated above the gel. (C) N-SART3-FLAG was transiently expressed in HeLa cells and immunoprecipitated with the anti-FLAG antibody. Co-precipitated complexes were eluted by the FLAG peptide and resolved by ultracentrifugation in 10-30% glycerol gradient. Proteins were isolated from individual fractions and SNRPB2 detected by western blotting.

Figure S3

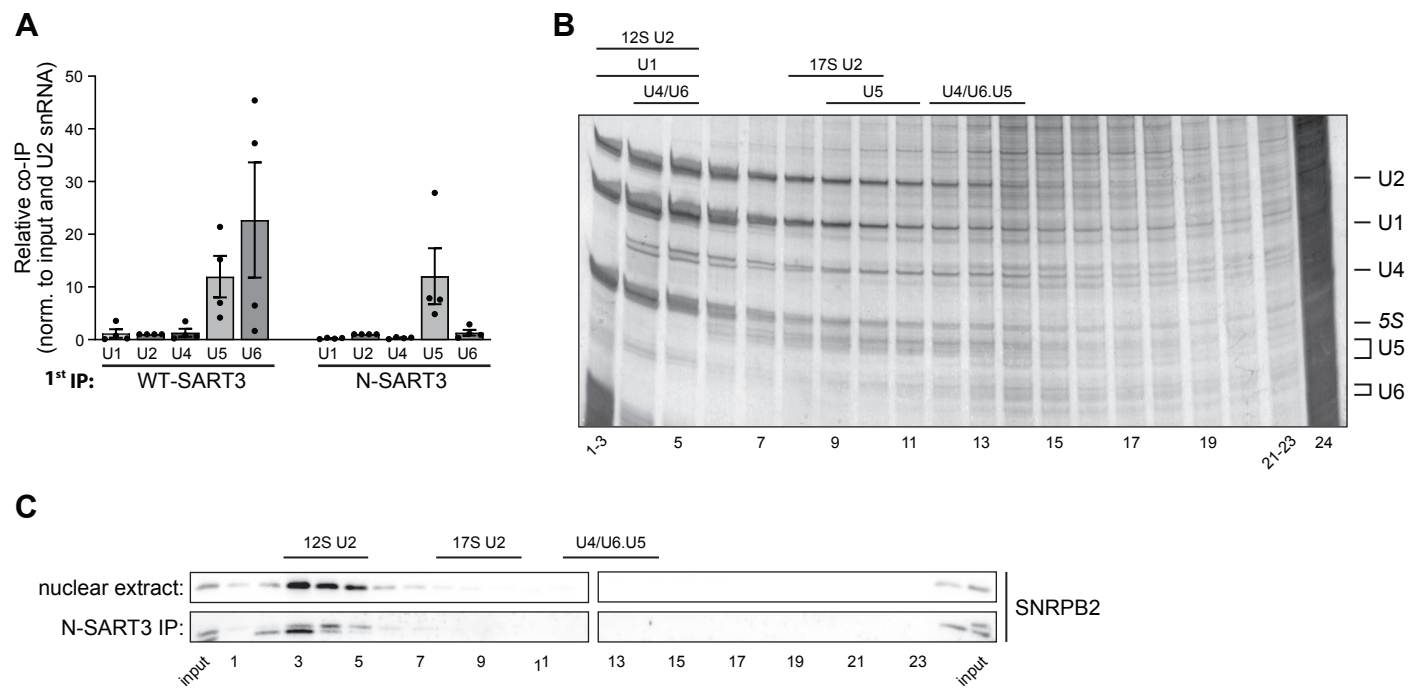

Fig. S3. snRNA detection in SART3-U2 complexes and monitoring distribution of snRNAs in glycerol gradient after ultracentrifugation. (A) snRNA co-purified by double immunoprecipitation with anti-GFP and anti-SNRPA1 antibodies were analyzed by RT-qPCR and double normalized to inputs and the U2 snRNA signal. (B) Nuclear extract was subjected to ultracentrifugation in 10-30% glycerol gradient, RNA from individual fractions isolated, resolved on denaturing UREA polyacrylamide gels and silver stained. Position of individual snRNP particles is indicated above the gel. (C) N-SART3-FLAG was transiently expressed in HeLa cells and immunoprecipitated with the anti-FLAG antibody. Co-precipitated complexes were eluted by the FLAG peptide and resolved by ultracentrifugation in 10-30% glycerol gradient. Proteins were isolated from individual fractions and SNRPB2 detected by western blotting.

Journal of Cell Science • Supplementary information

Fig. S4. Western Blot Transparency

Fig.1D

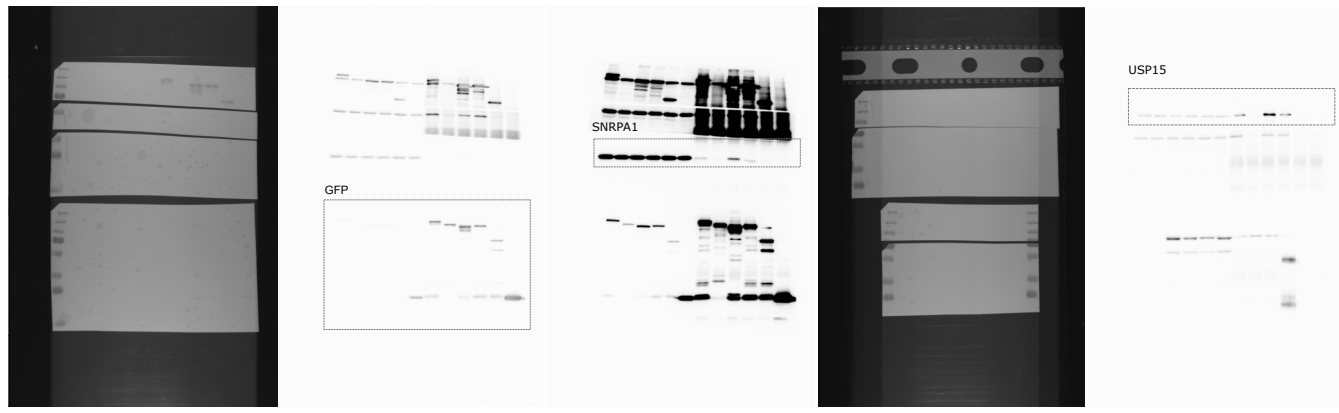

Fig.1E

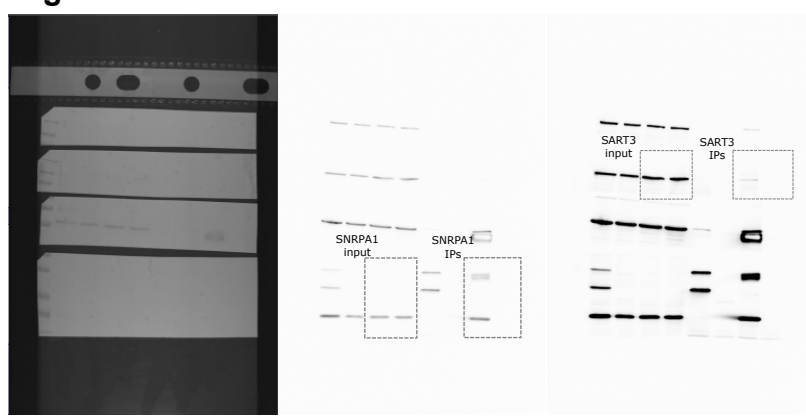

Fig.2A

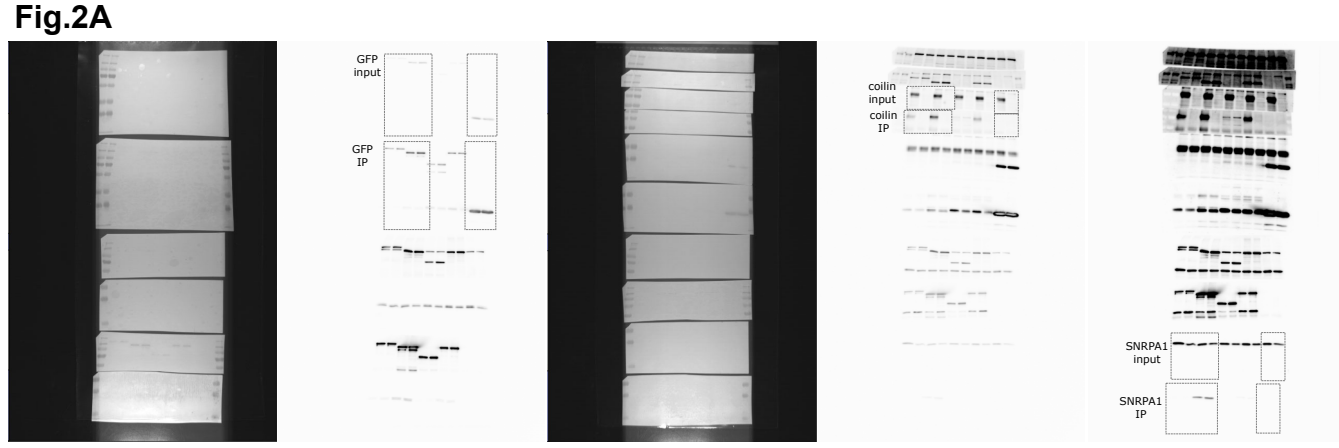

Fig.2B

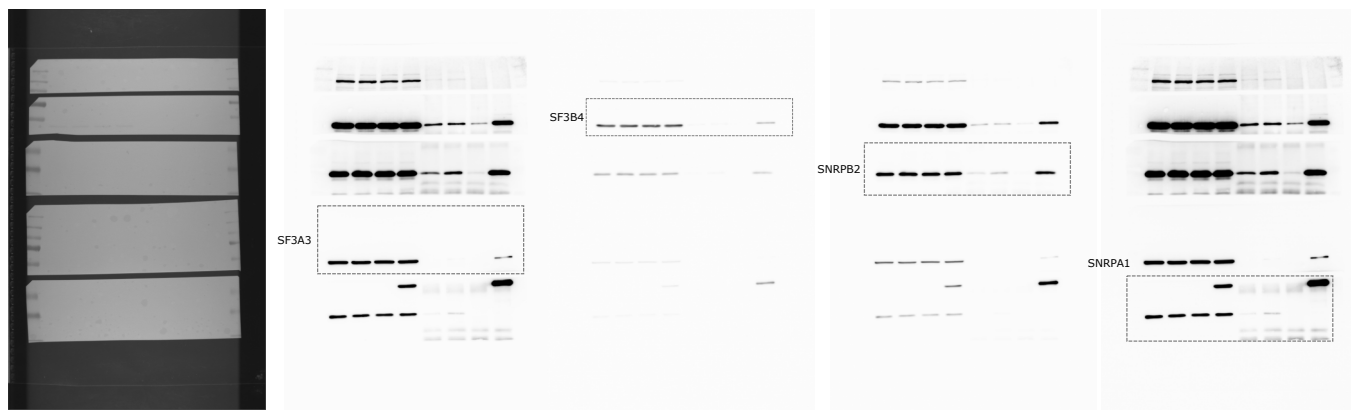

Journal of Cell Science • Supplementary information

Fig.2B - continued

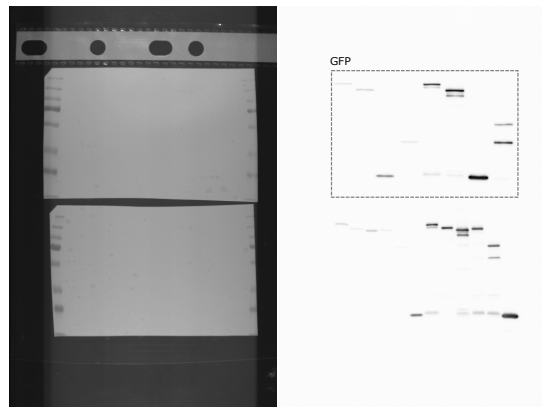

Fig.2C

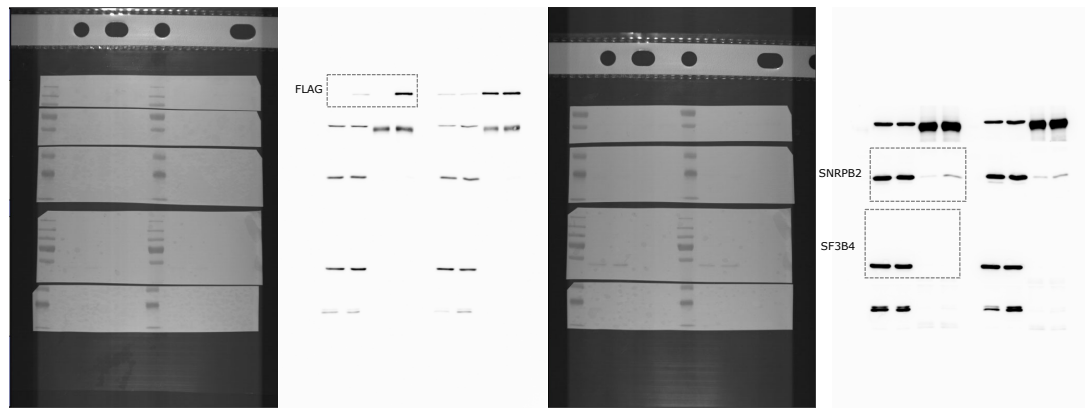

Fig.2D

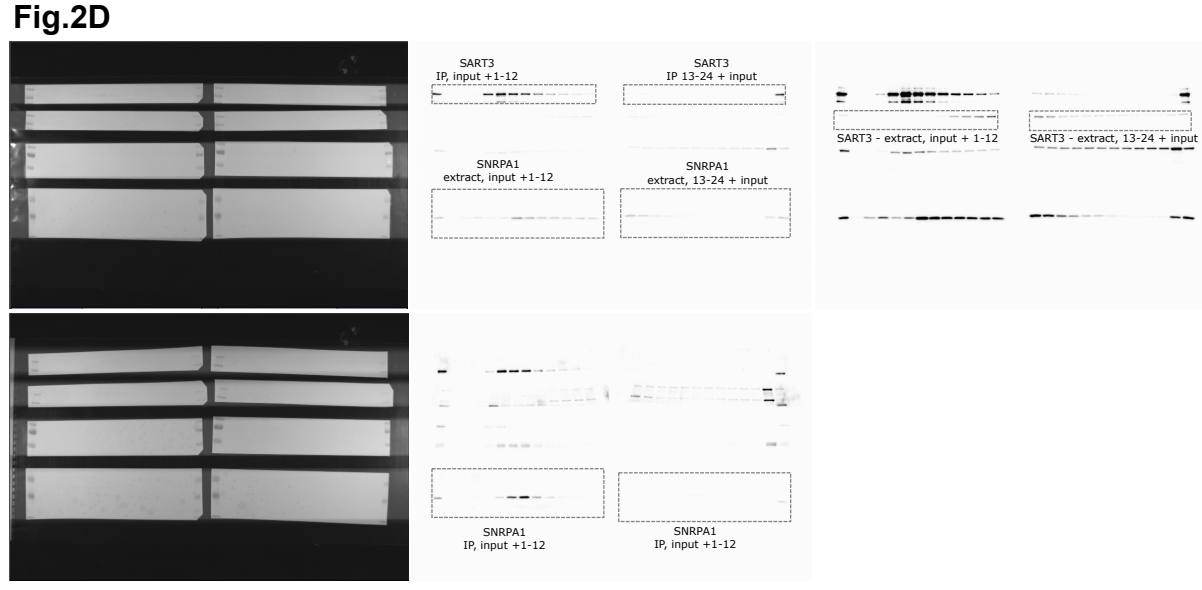

Fig.2E

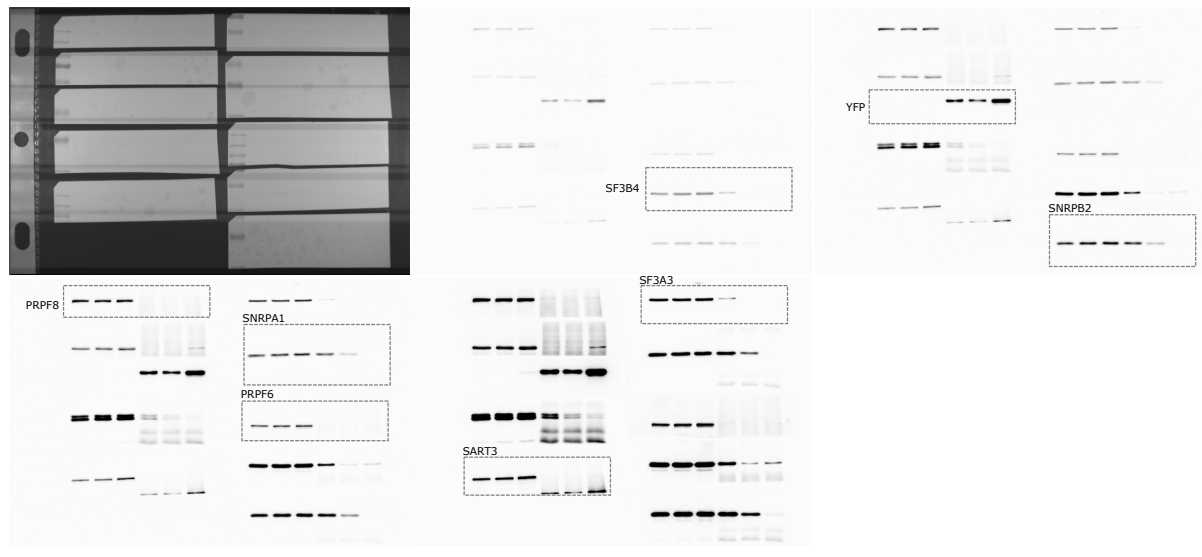

Journal of Cell Science • Supplementary information

Fig.3A

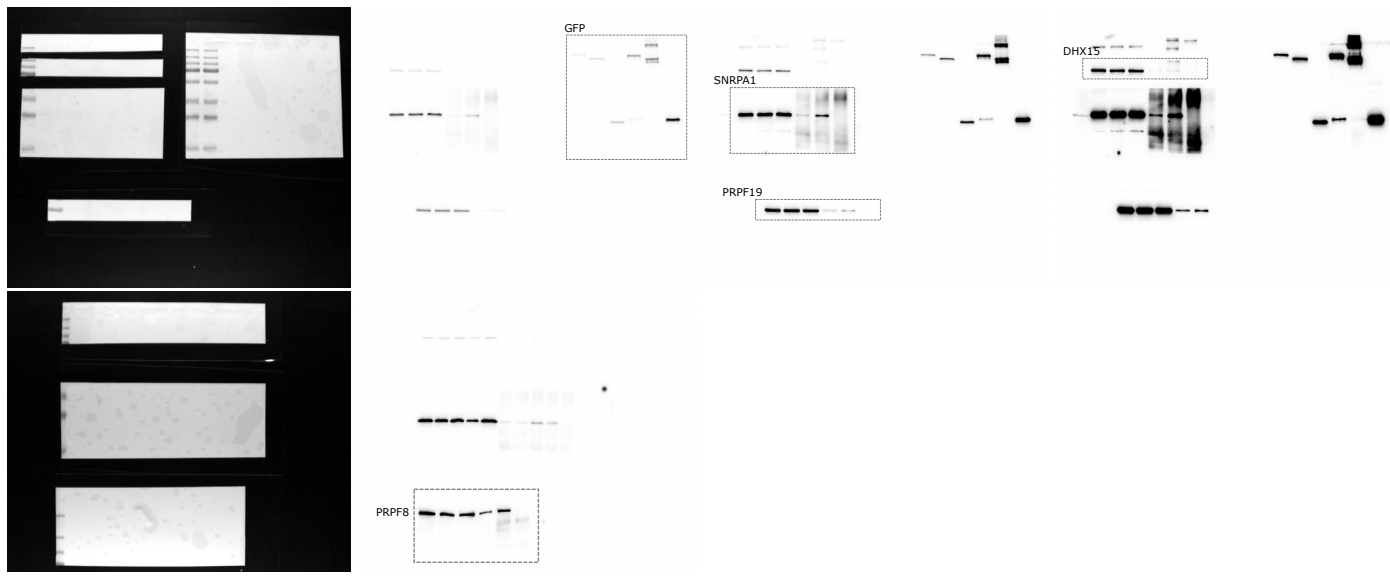

Fig.3B

Journal of Cell Science • Supplementary information

Fig.3D

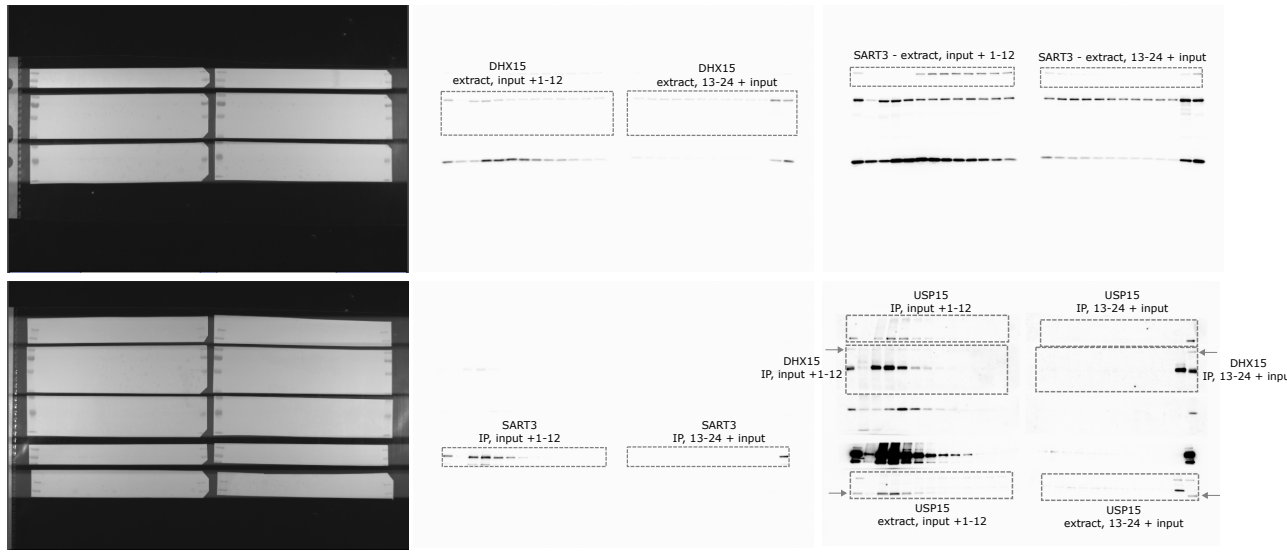

Fig.4A

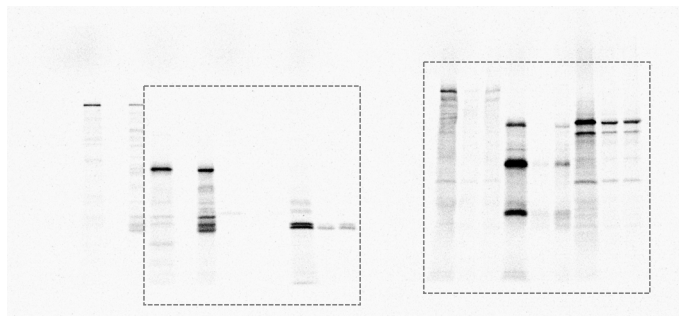

Fig.4B

Fig.4C

Journal of Cell Science • Supplementary information

Fig.4D

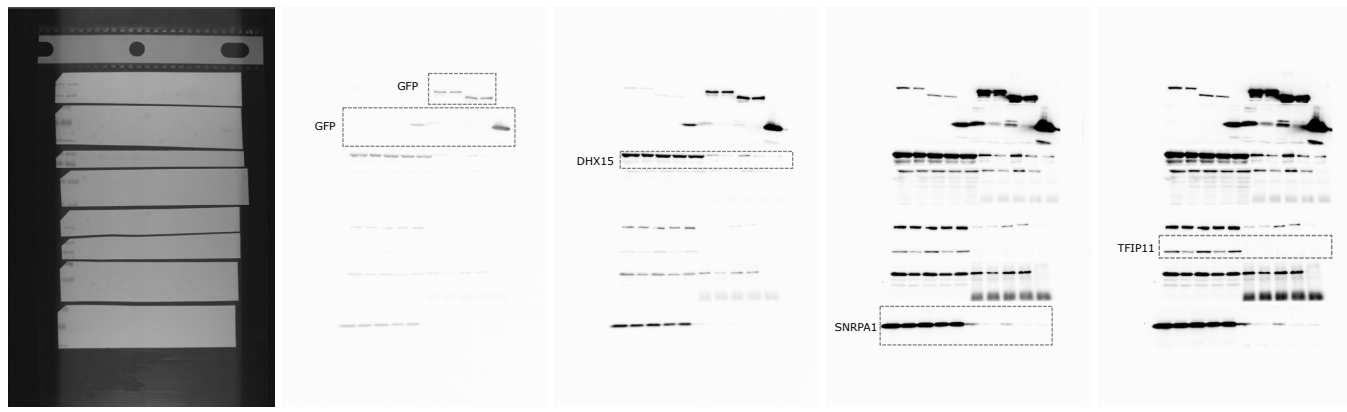

Fig.4E

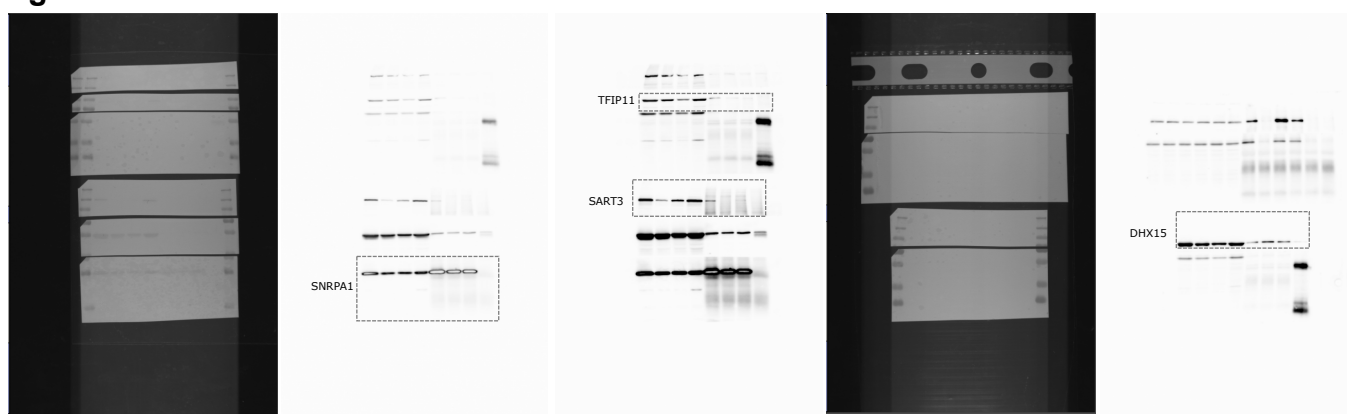

Fig.S1C

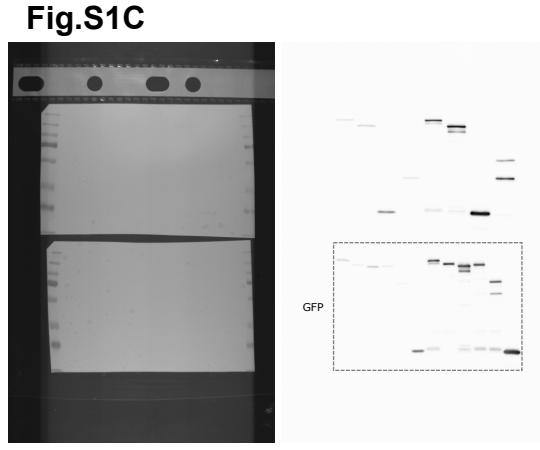

Fig.S2C

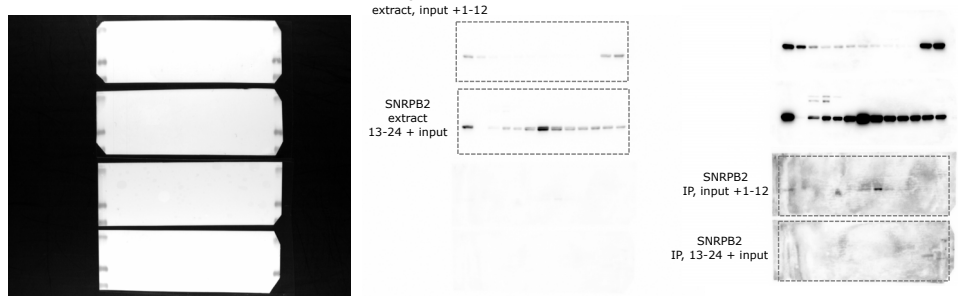

Fig.S3C

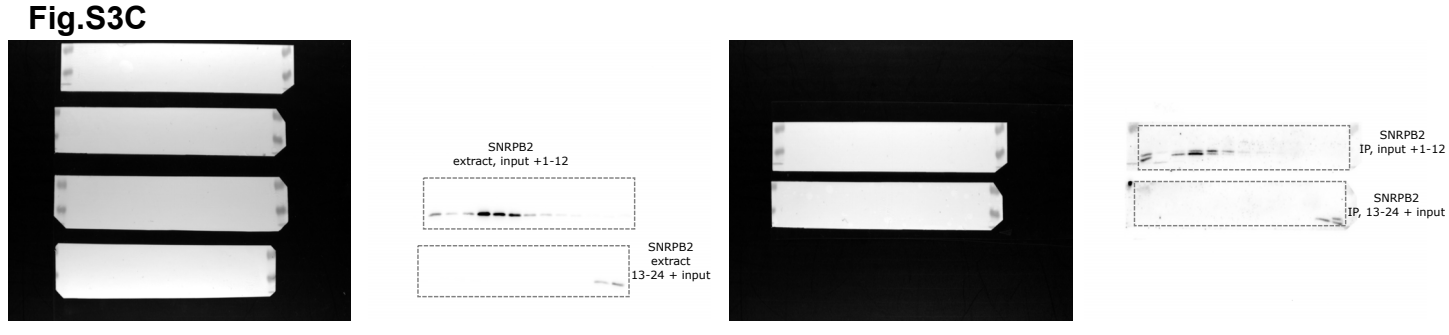

Journal of Cell Science • Supplementary information

Table S1. A list of primers

Cloning primers

ΔE-SART3-pEGFP-N1	F: 5‘-AACCAGCTGGAGATTGAGAGACTG-3‘ R: 5‘-CATGAGATCTGAGTCCGGTAGC-3‘
SART3-TEV-pEGFP-N1	F: 5‘-TTCCAGGGCGCCCGGGATCCACCGGTCGC-3‘ R: 5‘-GTACAGGTTCTCCCGCGGTACCGTCGACTGCA-3‘
N-SART3-pFLAG-C3	F: 5‘-GACGATGACAAGCAGTACTCAGATCTCATGGCGACTGCGGCCGAAACCT-3‘ R: 5‘-GATCCCGGGCCCGCGGTACCGTCGACTGCAGAAT-3‘
N-SART3-pDONR221	F: 5‘-GGGGACAAGTTTGTACAAAAAAGCAGGCTCGATGGCGACTGCGGCCGAA-3‘ R: 5‘-GGGGACCACTTTGTACAAGAAAGCTGGGTTATTACAGGGAGGCTGCCTTCTC-3‘
SNRPB2-pIVT	F: 5‘-GACCTCGAGATGGATATCAGACCAAATCATACAA-3‘ R: 5‘-GACGAATTCTTATTTCTTGGCATAGGTGATCTTC-3‘
SNRPA1-pIVT	F: 5‘-GACCTCGAGATGGTCAAGCTGACGGCG-3‘ R: 5‘-GACGAATTCTCAGGACCCGTTTGTGACTGTG-3‘

PCR primers for TnT templates

PRPF3-383-683-TnT	F: 5‘-TACGTAATACGACTCACTATAGGGAGAGCCACCATGGATATTCCTGAAATTGAGTGG-3‘ R: 5‘-GACGTCGACTCAATCAGTGGACTCTAACACAG-3‘
DHX15-TnT	F: 5‘-TACGTAATACGACTCACTATAGGGAGAGCCACCATGTCCAAGCGGCACCGGTTG-3‘ R: 5‘-GACGAATTCTCAGTACTGTGAATATTCCTTGGATTG-3‘
DHX15-1-320-TnT	F: 5‘-TACGTAATACGACTCACTATAGGGAGAGCCACCATGTCCAAGCGGCACCGGTTG-3‘ R: 5‘-TCACTCAACAGGATGTGTACGCCC-3‘
DHX15-288-795-TnT	F: 5‘-TACGTAATACGACTCACTATAGGGAGAgccaCCATGGTTATAGTTATGAGCGCTACTC-3‘ R: 5‘-GACGAATTCTCAGTACTGTGAATATTCCTTGGATTG-3‘

qPCR primers

U1 snRNA	F: 5‘-ATACTTACCTGGCAGGGGAG-3‘ R: 5‘-CAGGGGAAAGCGCGAACGCA-3‘
U2 snRNA	F: 5‘-CTCGGCCTTTTGGCTAAGAT-3‘ R: 5‘-CGTTCCTGGAGGTACTGCAA-3‘
U4 snRNA	F: 5‘-TGGCAGTATCGTAGCCAATG-3‘ R: 5‘-CTGTCAAAAATTGCCAGTGC-3‘
U5 snRNA	F: 5‘-CTCTGGTTTCTCTTCAGATC-3‘ R: 5‘-TGTTCCTCTCCACGGAAATC-3‘
U6 snRNA	F: 5‘-CGCTTCGGCAGCACATATAC-3‘ R: 5‘-AAAATATGGAACGCTTCACGA-3‘
ACTB spliced	F: 5‘-CGTGCGTGACATTAAGGAGA-3‘ R: 5‘-ACAGGACTCCATGCCCAG-3‘
ACTB unspliced	F: 5‘-AGCTAAGTCCTGCCCTCATT-3‘ R: 5‘-GTACAGGTCTTTGCGGATGT-3‘
ALDOA spliced	F: 5‘-TATCAAATCCAAGGGCGGTG-3‘ R: 5‘-GCTCCGTCCTTCTTGTACTG-3‘
ALDOA unspliced	F: 5‘-TATCAAATCCAAGGGCGGTG-3‘ R: 5‘-ATTCCCTGCCTCACTAACCT-3‘
B2M spliced	F: 5‘-AGATGTCTCGCTCCGTGG-3‘

	R: 5‘-CGTGAGTAAACCTGAATCTTTGG-3‘
B2M unspliced	F: 5‘-AGATGTCTCGCTCCGTGG-3‘ R: 5‘-CTTGGAGAAGGGAAGTCACG-3‘
GAPDH spliced	F: 5‘-ACATCGCTCAGACACCATGG-3‘ R: 5‘-GTTAAAAGCAGCCCTGGTGA-3‘
GAPDH unspliced	F: 5‘-CAGGGAAGCTCAAGGGAGAT-3‘ R: 5‘-GTTAAAAGCAGCCCTGGTGA-3‘
LDHA spliced	F: 5‘-TGGCAGCCTTTTCCTTAGAA-3‘ R: 5‘-CTTTCTCCCTCTTGCTGACG-3‘
LDHA unspliced	F: 5‘-TGGCAGCCTTTTCCTTAGAA-3‘ R: 5‘-TGTGCAACTGCACTCTACCC-3‘
PGK1 spliced	F: 5‘-ACAACCAGATAACAAACAACCAG-3‘ R: 5‘-GAGTACTTGTCAGGCATGGG-3‘
PGK1 unspliced	F: 5‘-TGTTGTCTCTCTTTGGTTGCA-3‘ R: 5‘-GAGTACTTGTCAGGCATGGG-3‘
RPL19 spliced	F: 5‘-ATGCCAGAGAAGGTCACATG-3‘ R: 5‘-CACATTCCCCTTCACCTTCA-3‘
RPL19 unspliced	F: 5‘-ATGCCAGAGAAGGTCACATG-3‘ R: 5‘-ACTAGCCATCAAAGCAGCAA-3‘